broad nasal bridge, long palpebral fissures, and a tented mouth, as well as some degree of brachytelephalangy [Horn et al., 2011]. Variable neurological abnormalities, including seizures and muscular hypotonia, were also associated with this condition. Extensive biochemical analysis showed that hyperphosphatasia was unlikely to be the result of increased activity of osteoblastic cells or hepatobiliary dysfunction, and the causes of HPMRS were unknown [Kruse et al., 1988].

In 2010, Krawitz et al. performed whole-exome sequencing of three siblings with HPMRS (OMIM 239300) and identified homozygous or compound heterozygous mutations in *PIGV* in a total of six families with HPMRS [Krawitz et al., 2010]. *PIGV* encodes a molecule that acts as the second mannosyltransferase in the glycosylphosphatidylinositol (GPI) anchor biosynthesis pathway. Subsequently, mutations in *PIGO, PGAP2, PGAP3*, and *PIGW*, which are also involved in GPI biosynthesis, have been identified in individuals with HPMRS (OMIM 614749, OMIM 614207, OMIM 615716, and OMIM 610275, respectively) [Krawitz et al., 2012, 2013; Hansen et al., 2013; Chiyonobu et al., 2014; Howard et al., 2014]. In this study, we performed whole-exome sequencing of a family with HPMRS but without mutations in *PIGV* and *PIGO* and identified compound heterozygous mutations in *PIGL*.

MATERIAL AND METHODS

Exome Sequencing

DNA was extracted using a standard protocol from blood samples of an affected female and her parents. Control DNA was obtained from 192 healthy Japanese individuals. This study was approved by the Ethics Committee of Tohoku University School of Medicine. We obtained informed consent and specific consent for photographs from the parents of the affected individual.

Exome sequencing was conducted on an individual with HPMRS. Targeted enrichment was performed using the SureSelect Human All Exon V2 kit. Exon-enriched DNA libraries were sequenced on the Illumina Hiseq 2000 for 101 bp. Burrows-Wheeler Aligner (BWA) was used to align the sequence reads to the human genome (hg19); all parameters of BWA were kept at the default settings. Following removal of duplicates from the alignments, realignment around known indels, recalibration, and SNP/indel calling were performed with Genome Analysis Toolkit (GATK, 1.5) [McKenna et al., 2010]. ANNOVAR was used for the annotation against the RefSeq database and dbSNP [Wang et al., 2010].

Sanger Sequencing

Each exon with flanking intronic sequences in *PIGV, PIGO, PIGN, PIGB*, and *PIGL* was amplified with primers based on GenBank sequences (NM_017837.2, NM_152850.3, NM_176787.4, NM_004855.4, and NM_004278.3, respectively). The M13 reverse or forward sequence was added to the 5′ end of the polymerase chain reaction (PCR) primers for use as sequencing primers. PCR was performed in 15 μl of solution containing 67 mM Tris–HCl (pH 8.8), 6.7 mM $MgCl_2$, 17 mM NH_4SO_4, 6.7 μM EDTA, 10 mM β-ME, 1.5 mM dNTPs, 10% (v/v) DMSO, 1 μM of each primer, 25 ng genomic DNA and 1 U of Taq DNA polymerase. The reaction consisted of 37 cycles of denaturation at 94°C for 20 sec, annealing at the indicated temperature for 30 sec and extension at 72°C for 30 sec. PCR products were purified using MultiScreen PCR plates (Millipore, Billerica, MA). The purified products were sequenced on an ABI 3500xL Genetic Analyzer (Applied Biosystems, Foster City, CA).

For subcloning, PCR products of exon 1 and 2 in *PIGL* were subcloned using a pTOPO TA cloning kit (Invitrogen, Carlsbad, CA) and transformed in TOP10F competent cells (Invitrogen). Plasmids were purified from each colony and sequenced.

Flow Cytometry

Surface expression of GPI-anchored proteins (GPI-APs) of granulocytes was determined by staining cells with PE-conjugated mouse anti-human CD59 (H19), anti-human DAF (IA10), anti-human CD24 (ML5), anti-human CD16 (3G8) antibodies, each isotype IgG (BD Biosciences, Franklin Lakes, NJ) and Alexa 488-conjugated inactivated aerolysin (FLAER; Protox Biotech, Canada). CD59, DAF, CD24, and CD16 are GPI-APs and FLAER binds to surface GPI-APs. The surface expression was then analyzed using a flow cytometer (Canto II; BD Biosciences) and FlowJo software (Tommy Digital, Inc., Tokyo, Japan).

Functional Analysis

PIGL-deficient CHO cells (M2S2) [Nakamura et al., 1997] were transiently transfected with *PIGL* cDNA that was driven by the strong SRα promoter (pME hPIGL-HA or pME HA-hPIGL). Two days later, cells were stained with anti-CD59, anti-DAF and FLAER and analyzed by flow cytometry. Lysates were separated using SDS–PAGE and Western blotting was performed.

RESULTS

Clinical Report

The patient was the first child of healthy and non-consanguineous Japanese parents. She was born at 33 weeks and 3 days of gestation by caesarean because of maternal infection. Her weight and height at birth were 2,510 g and 51 cm, respectively. She was treated with oxygen inhalation for several days because of transient tachypnea. She was suspected as having Beckwith–Wiedemann syndrome because of hypotonia, a large tongue, separation of the rectus abdominis muscle, and coarse facial features.

At 4 months of age, the patient's serum levels of ALP were found to be extremely high at 4,394 IU/L (Normal, 395–1,289 IU/L) and she was referred to our hospital. A radiograph of her hands showed a slight delay of bone maturation and slight dilation of the ulnar metaphysis. Alpha D3 administration was started at 5 months and ended at 1 year and 8 months of age. Laboratory investigations for inborn errors of metabolism, including toluidine blue staining in a urine sample, glycosaminoglycan in the urine, and lysosome enzymes, were normal. Karyotyping analysis on cultured leukocytes and subtelomere MLPA, FISH for 17p11.2 detecting Smith–Magenis syndrome, and array CGH analysis were all normal.

Twitching of the extremities with epileptic discharge on EEG started at 4 months of age and required anti-convulsant therapy. Brain CT and MRI showed dilatation of the bilateral lateral ven-

tricles, third and fourth ventricles and sub-arachnoid space, as well as hypoplasia of the cerebellar vermis. She was suspected as having mild deafness (right: 30 dB and left 45 dB).

At 1 year and 10 months, her weight and height were 7.9 kg (−2 SD) and 80 cm (−1 SD), respectively. Her craniofacial features included midface hypoplasia, hypertelorism, long palpebral fissures, strabismus, depressed nasal bridge, anteverted nostrils, tented upper lip vermilion, full cheeks, a high palate, and ear anomalies (Fig. 1A). Teeth eruption was not observed. In the extremities, the 2nd and 3rd digits were overlapping. The terminal phalanges of the hands and feet were short with hypoplastic nails. Her development was as follows: head control at 5 months, crawling at 1 year and 7 months, sitting at 2 year and 3 months, and walking while holding onto something at 2 years and 7 months. At 3 years and 6 months, she was unable to walk independently, and speech development was markedly delayed. ALP remained persistently elevated (3,000–4,500 U/L, Fig. 1B).

Molecular and Biochemical Analysis

Mutation screening for genes in GPI biosynthesis showed that no mutations were identifiable by Sanger sequencing analysis in any exons coding for *PIGV, PIGO, PIGN,* and *PIGB.* We then performed exome sequencing with a sample from the proband. Using the sequencing analysis pipeline from BWA and GATK, we identified approximately 8,883 nonsynonymous, nonsense, splicing site variations, coding insertions, and/or deletions (indels) per individual. Filtering steps using variant databases (dbSNP132, the 1,000 Genome Project database and ESP 5,400) resulted in the identification of 216 variants. Two frameshift mutations in *PIGL* (c.36_48del [p.Leu13Alafs*11] and c.254_255del [p.Glu86Aspfs*2]) were detected as variants in genes that participate in the GPI-anchor biosynthesis (hsa00563) and the GPI-anchor biosynthesis (hsa00563)/metabolic pathway (hsa00110) in KEGG pathway, respectively. Sanger sequencing validated the heterozygous state of the two variants in *PIGL* (Fig. 2A). Two variants resulted in a premature termination and it was assumed that truncated proteins were produced (Fig. 2B).

Subcloning of PCR products of exons 1 and 2 from parental samples followed by sequencing showed that the father was heterozygous for c.36_48del and the mother was heterozygous for c.254_255del in *PIGL*, thus confirming the compound heterozygosity in the affected individual (Fig. 2A).

The c.36_48del and c.254_255del in *PIGL* were not reported in dbSNP132, the 1,000 Genome Project database or in ESP 5,400. c.254_255del, and not c.36_48del, was reported in one in 1,000 Japanese exomes (http://www.genome.med.kyoto-u.ac.jp/SnpDB/) and identified in 1 in 192 of our in-house Japanese controls in a hetrozygous manner, suggesting that c.254_255del could be identified at a frequency of 1:200–1:1000 in Japanese people.

These genomic analyses suggested that the patient has *PIGL*-deficiency, which is one of the inherited GPI deficiencies. More than 100 mammalian proteins are modified by a GPI anchor at their C terminus [Krawitz et al., 2010]. The expression of GPI-APs have been decreased in other inherited GPI deficiencies [Maydan et al., 2011; Chiyonobu et al., 2014; Howard et al., 2014]. To examine if the GPI-APs decreased in cells from our patient, peripheral blood cells were analyzed by flow cytometry. Surface expression of various GPI-APs on the granulocytes from the patient (Fig. 3, thick lines) was severely decreased (2% of the control in CD16 expression) compared with that from the normal samples (dotted lines).

PIGL-deficient CHO cells (M2S2) [Nakamura et al., 1997] were transiently transfected with wild type (Fig. 4, dotted line),

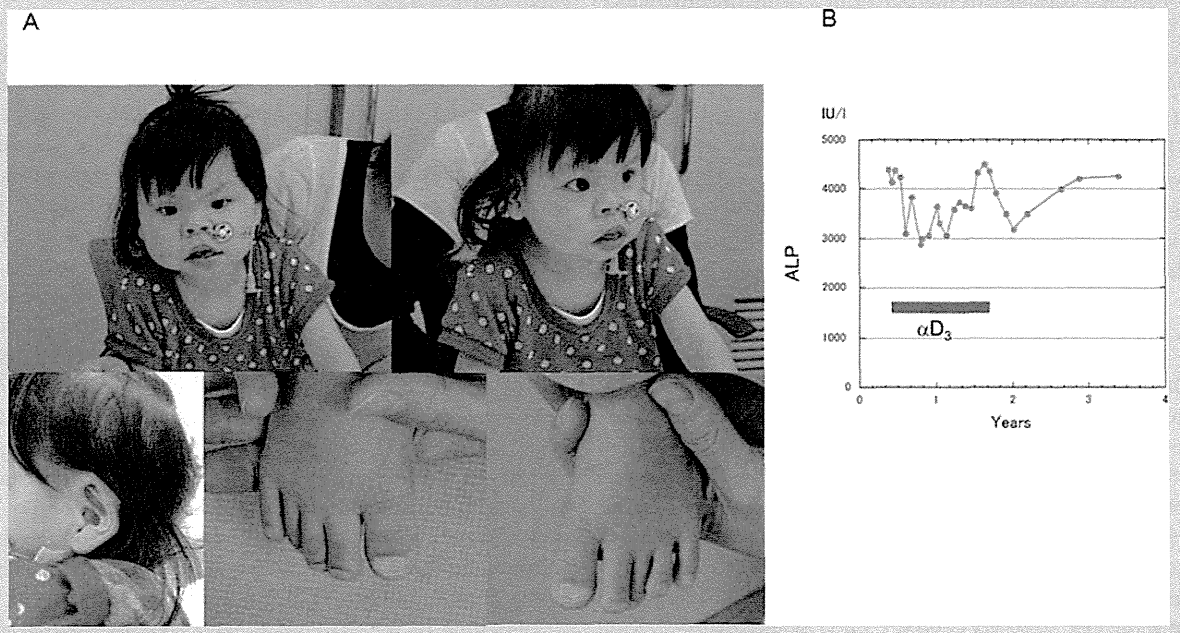

FIG. 1. Clinical manifestation of the proband. A: Photos of the girl at 2 years and 7 months of age. B: Serum levels of ALP in the patient.

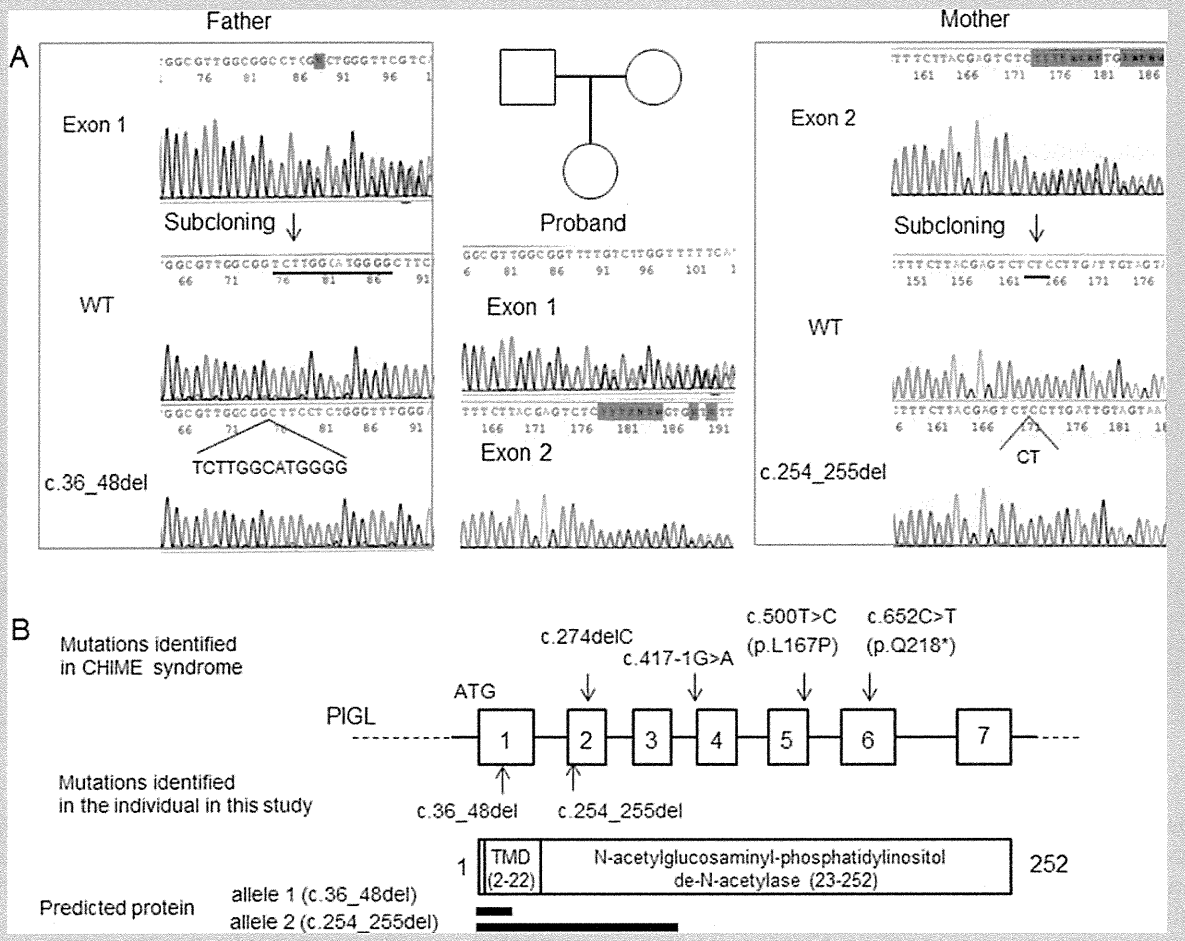

FIG. 2. Sanger sequencing of the family. A: Mutation analysis of the individual and her parents. B: The genomic structure of *PIGL* and mutations identified in CHIME syndrome and this study.

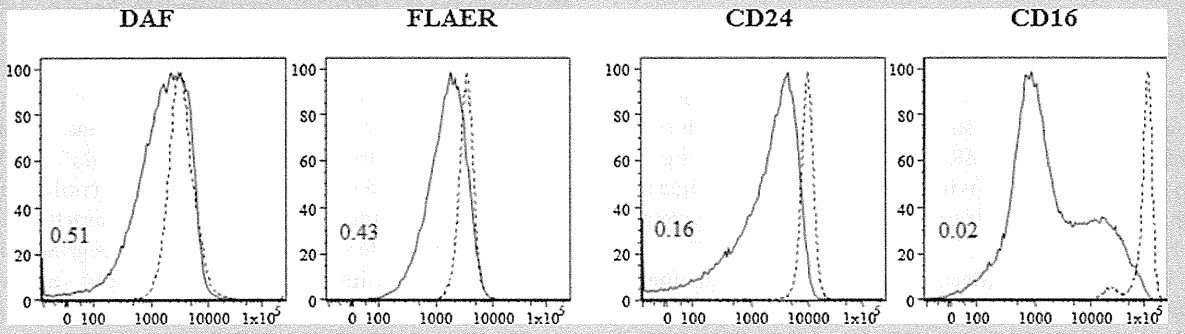

FIG. 3. Flow cytometry of granulocytes. Surface expression of various GPI-APs on the granulocytes from the patient (thick lines) was severely decreased compared with that from the normal samples (dotted lines). Light shadows are isotype controls. The value of the mean fluorescent intensity of each sample against normal is shown in each panel.

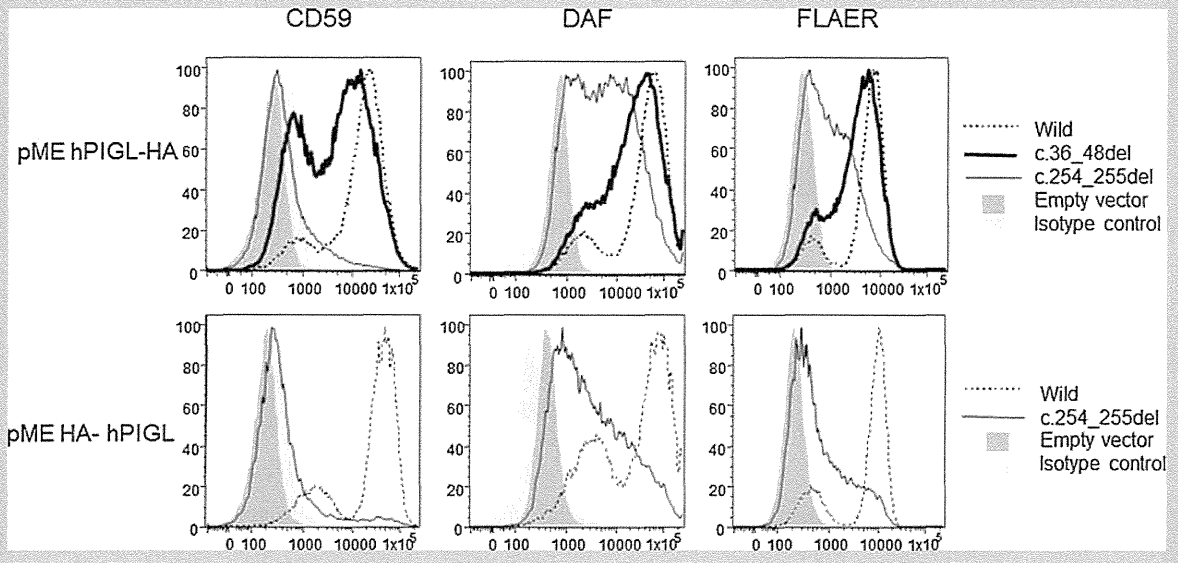

FIG. 4. PIGL-deficient CHO cells (M2S2) [Nakamura et al., 1997] were transiently transfected with wild type (dotted line), the c.36_48del mutant (thick line), or the c.254_255del mutant (thin line) PIGL cDNA that was driven by the strong SRα promoter (pME hPIGL-HA or pME HA-hPIGL) with an HA-tag at the C-(upper panels) or N-terminus (lower panels). Two days later, cells were stained with anti-CD59, anti-DAF and FLAER and analyzed by flow cytometry. The gray shadow denotes empty vector transfections; light gray shadows are isotype controls.

c.36_48del mutant (thick line) or c.254_255del mutant (thin line) *PIGL* cDNA with an HA-tag at the C-terminus (upper panels) or at the N-terminus (lower panels). Both mutants could only partially restore the surface expression of GPI-APs. The activity of the c.254_255del mutant was severely affected, and the N-terminal tagged construct had almost no activity. These results suggested that the remaining activity was not due to the truncated proteins. Faint bands (* and **) could be detected in the lysate of C-terminally tagged c.36_48 mutant transfected cells (Fig. 5A), which corresponded to the isoforms starting at the downstream methionines (2 and 3 of Fig. 5B) that showed residual PIGL activity. No band could be detected from the lysate of the c.256_255 mutant tagged at either terminus (data not shown).

DISCUSSION

We report on the case of a girl with distinctive facial features, severe intellectual disability, and persistent increased serum levels of ALP who was diagnosed with HPMRS. Whole-exome sequencing identified two frameshift mutations in *PIGL*, which were inherited from the father and mother, suggesting that *PIGL* mutations are responsible for HPMRS.

Many eukaryotic cell surface proteins are bound to the cell membrane by a GPI-anchor. More than 20 different gene products are involved in GPI biosynthesis [Fujita and Kinoshita 2012]. Recent studies revealed that genetic defects in various components of the GPI-anchor biosynthesis pathway cause inherited GPI deficiencies. Somatic mutations in *PIGA* in hematopoietic stem cells cause paroxysmal nocturnal hemoglobinuria [Ware et al., 1994]. A promoter mutation in *PIGM* causes portal venous thrombosis and absence seizures [Almeida et al., 2006]. Germline mutations in *PIGN* and *PIGA* cause congenital anomalies with hypotonia and seizures [Maydan et al., 2011; Johnston et al., 2012]. Germline mutations in *PIGV*, *PIGO*, *PGAP2*, *PGAP3*, and *PIGW* have been identified in individuals with HPMRS [Krawitz et al., 2010, 2012, 2013; Chiyonobu et al., 2014; Howard et al., 2014]. Recently, mutations in *PIGT* have been identified in a family with intellectual disability [Kvarnung et al., 2013]. Thus, the clinical spectrum of disorders caused by the GPI-anchor deficiency has expanded.

PIGL encodes a 252 amino acid endoplasmic reticulum (ER) protein, located on the ER membrane with one transmembrane region and most of the protein located on the cytoplasmic side [Nakamura et al., 1997]. PIGL is involved in the second step of GPI biosynthesis, which is de-N-acetylation of N-acetylglucosaminyl-phosphatidylinositol (GlcNAc-PI). Following de-N-acetylation, glucosaminyl-phosphatidylinositol (GlcN-PI) flips to the luminal side of ER where GlcN-PI undergoes further extensions followed by its transfer to acceptor proteins [Nakamura et al., 1997; Watanabe et al., 1999]. Mutations in *PIGL* have been identified in CHIME syndrome, an autosomal recessive disorder characterized by colobomas, congenital heart defects, early onset migratory ichthyosiform dermatosis, intellectual disability, and ear anomalies, including conductive hearing loss [Ng et al., 2012]. Our patient manifested severe intellectual disability, seizures, ear anomalies, and feeding difficulties, which overlapped with symptoms of CHIME syndrome [Ng et al., 2012]. However, our patient did not have colobomas, congenital heart defects, early onset migratory ichthyosiform, or genitourinary abnormalities. Inherited GPI

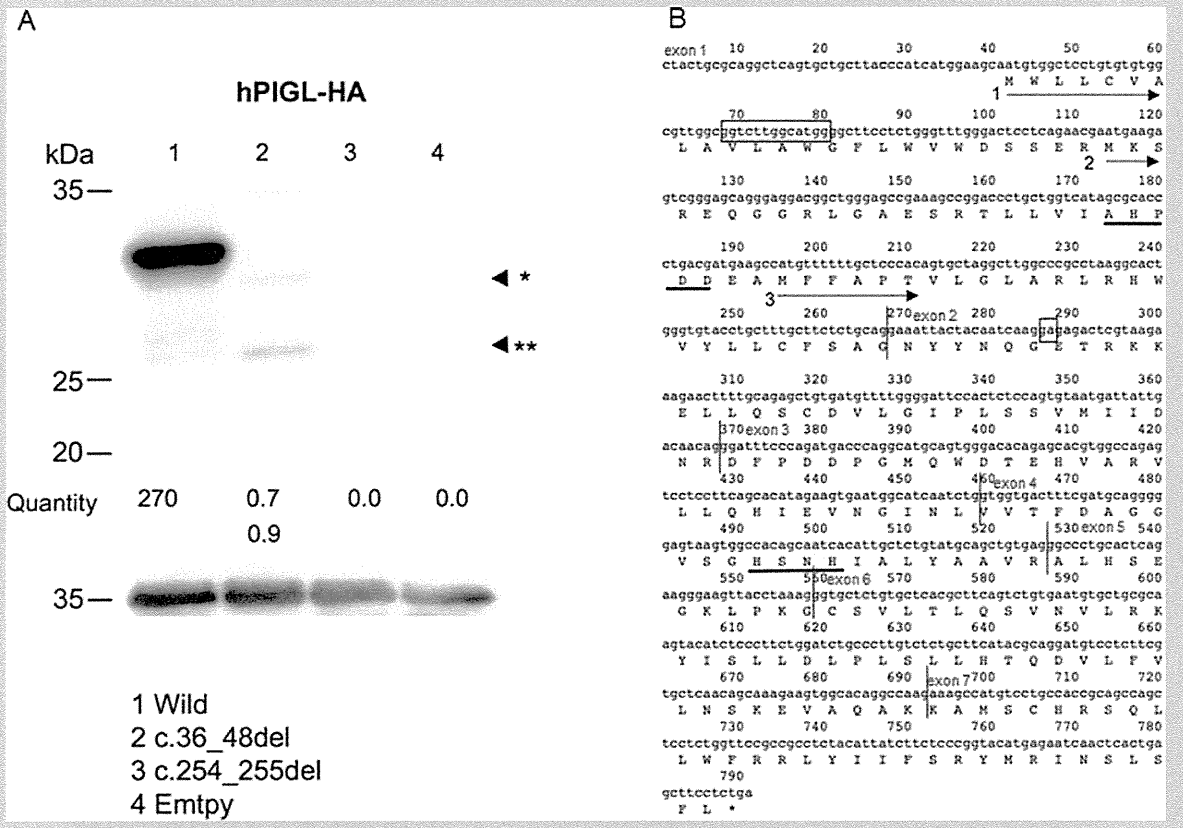

FIG. 5. Functional analysis. A: Lysates were separated by SDS–PAGE and western blotting was performed. Faint bands (* and **) could be detected from the lysate of the C-terminally tagged c.36_48 mutant transfected cells, which corresponded to the isoform starting from the down stream methionines (2 and 3 in Fig. 5B) that showed residual *PIGL* activity. No band could be detected from the lysate of the c.256_255 mutant tagged at either terminus. (Normalized with the intensities of GAPDH, the loading control, and luciferase activities used for evaluating transfection efficiencies). B: The sequence of *PIGL* cDNA; thick lines, conserved motifs; numbered arrows, three translation initiation sites; boxes, deletions in this patient.

deficiencies caused by a defect in the GPI-biosynthesis genes should show similar symptoms that result from the decreased expression of various GPI-APs on the cell surface. The severity depends on the amount of the GPI-anchor produced in ER, and the individual's genetic background may also have some influence on variations. Clinical manifestations in our patient were more similar to those in individuals with HPMRS, including hypertelorism, long palpebral fissures, broad nasal tip, tented upper lip, brachytelephalangy, severe intellectual disability and persistent hyperphosphatasia (Table I) [Horn et al., 2011]. These results suggest that frameshift mutations in 5′ terminus of *PIGL* cause HPMRS. It is possible that *PIGL* mutations identified in patients with CHIME syndrome might have higher residual activities.

Brain CT and MRI of our patient showed cerebellar atrophy. Frontotemporal atrophy and cerebellar hypoplasia have been shown in patients with *PIGT* mutations [Kvarnung et al., 2013]. Cerebral and cerebellar atrophy have been reported in a patient with *PIGO* mutation [Nakamura et al., 2014] and in patients with *PIGN* mutations [Maydan et al., 2011; Ohba et al., 2014], suggesting that cerebral atrophy and cerebellar atrophy are common features in patients with inherited GPI deficiencies. It is of note that cerebral atrophy has been also observed in patients with CHIME syndrome [Shashi et al., 1995; Schnur et al., 1997].

Our previous study demonstrated that mutant CHO cells having defects in the later step genes efficiently secrete ALP into the medium, whereas most ALP produced in the early step mutants is degraded in the cells [Murakami et al., 2012] because GPI transamidase is activated through binding with a mannose-containing GPI intermediate before this enzyme complex processes the precursor proteins for release. However, there are cases that are inconsistent with these experimental results. Some *PIGA*-deficient patients showed mild elevation of ALP (412 IU/L, normal range, 39–117 IU/L) [Johnston et al., 2012]. Elevation of ALP has not been reported in previously reported patients with *PIGL* deficiencies [Ng et al., 2012]. There may be differences in in vitro culture and in vivo body conditions; however, the primary reason for these differences needs to be identified in the future.

TABLE I. Summary of Clinical Features in Our Patient and HPMRS Patients With *PIGV*, *PIGO*, *PGAP2*, *PGAP3*, and *PIGW* Mutations

	Our study (PIGL)	PIGV	PIGO	PGAP2	PGAP3	PIGW
References		Horn et al. [2011]; Krawitz et al. [2010, 2012]	Krawitz et al. [2012]	Krawitz et al. [2013]; Hansen et al. [2013]	Howard et al. [2014]	Chiyonobu et al. [2014]
Sex	1 female	9 females and 5 males	3 females	4 female and 1 male	4 females and 2 males	1 proband
Age at assessment	1 year 10 months	7 months–17 years	20 months–15 years	3.5 and 28 years	2–17 years	ND
Origin	Japanese	German, Moroccan, Dutch, Polish, British, and European American	European	Finnish, Turkish, Northwestern Syria and Pakistani	Pakistani, American and Saudi–Arabian	Japanese
Height	−1.0 SD	normal in 13/14	−1.4 to −4.2 SD	−0.9 to 0.6 SD	normal in 4/5	ND
Weight	−2.0 SD	normal in 13/14	+0.6 to −3.3 SD	−1.0 SD to normal	normal in 4/5	ND
OFC	−1.0 SD	normal in 12/14	+0.7 to −5.5 SD	−4.5 SD to normal	−3.0 SD to normal	ND
Hyperphosphatasia	+	14/14	3/3	4/4	5/5	+
Intellectual disability	severe	14/14	3/3	4/4	5/5	+
Age at walking	delayed	delayed	delayed	5/5	delayed unable to walk in 4/5	ND
Delayed speech and language development	+	14/14	3/3	4/5	5/5 (none)	+
Muscular hypotonia	+	11/12	3/3	4/5	5/5	ND
Seizures	+	9/12	1/3	2/5	4/5	+
Apparent hypertelorism	+	+	3/3	1/2	5/5	ND
Long palpebral fissures	+	+	3/3	1/2		ND
Broad nasal tip	+	+	3/3	2/2	5/5	+
Tented upper lip vermilion	+	+	3/3	1/2	5/5	+
Brachytelephalangy	+	14/14	3/3	1/2	0/5	−
Anorectal abnormalities and/or constipation	−	6/12	3/3	1/2	ND	−
Aganglionic megacolon	−	2/14	1/3	1/2	ND	−
Heart defect	−	1/14	+	1/2	ND	−
Cleft palate	−	3/14	0/3	1/2	ND	−
Hearing impairment	+	3/14	0/3	1/2	ND	ND

ND, not described.

FACS analysis of granulocytes from our patient demonstrated severely decreased expression of GPI-APs. Functional analysis using *PIGL*-defective CHO cells revealed that the isoforms starting from the downstream methionines showed residual PIGL activity. It has been reported that two well-conserved motifs are essential for PIGL activity (Fig. 5B underlines). Two faint bands corresponding to the sizes of these isoforms were detected by western blot; the bigger band had both motifs but not the N-terminal transmembrane region. These two translation start sites do not fit well with Kozak's rule; therefore, these isoforms were not detected in the wild-type cells.

Severely decreased expression of GPI-APs in granulocytes of the patient suggest that these mutations in *PIGL* are associated with decreased GPI biosynthesis. Previous studies showed that the disruption of *PIGL* caused lethality in Saccharomyces cerevisiae [Watanabe et al., 1999], suggesting that PIGL has been considered as the only enzyme to catalyze the second step of GPI biosynthesis in yeast. Although the disease mechanims remain unknown, it is possible that a truncated protein translated from the allele with c.254_255del or C-terminal protein isoforms shown in our functional analysis using CHO cells might have the minimal residual activity of PIGL.

In conclusion, we identified compound heterozygous deletions in *PIGL* in a patient with distinctive facial appearance, developmental delay, intellectual disability, brachytelephalangy, and hyperphosphatasia. The clinical features were similar to those of HPMRS caused by mutations in *PIGV*, *PIGO*, *PGAP2*, *PGAP3*, and *PIGW*. Our findings will broaden the clinical spectrum of disorders with defects in the GPI biosynthesis pathway.

ACKNOWLEDGMENTS

The authors thank the patient's family who participated in this study. We are grateful to Prof. Shinji Nakao (Kanazawa University, Japan) for his valuable discussion, Yoko Tateda, Kumi Kato, Riyo Takahashi, Miyuki Tsuda, Nozomi Koshita, Mami Kikuchi, Kiyotaka Kuroda, and Kana Miyanagi for their technical assistance. We also acknowledge the support of the Biomedical Research Core of Tohoku University Graduate School of Medicine. This work was supported by a grant of Research on Applying Health Technology provided by the Ministry of Health, Labor and Welfare of Japan to Y.Ma. and Y.A. and a Grant-in-Aid for Scientific Research from the Japan Society for the Promotion of Science (C: 25461535) to I.F. This work was supported by a Grant-in-Aid for Scientific Research from the Japan Society for the Promotion of Science (C: 23590363); the Takeda Science Foundation; a Grant-in-Aid for Scientific Research on Innovative Areas (Exploring molecular basis for brain diseases based on personal genomics) from the Ministry of Education, Culture, Sports, Science, and Technology of Japan (25129705) to Y.Mu. and T.K.

REFERENCES

Almeida AM, Murakami Y, Layton DM, Hillmen P, Sellick GS, Maeda Y, Richards S, Patterson S, Kotsianidis I, Mollica L, Crawford DH, Baker A, Ferguson M, Roberts I, Houlston R, Kinoshita T, Karadimitris A. 2006. Hypomorphic promoter mutation in PIGM causes inherited glycosylphosphatidylinositol deficiency. Nat Med 12:846–851.

Chiyonobu T, Inoue N, Morimoto M, Kinoshita T, Murakami Y. 2014. Glycosylphosphatidylinositol (GPI) anchor deficiency caused by mutations in PIGW is associated with West syndrome and hyperphosphatasia with mental retardation syndrome. J Med Genet 51:203–207.

Fujita M, Kinoshita T. 2012. GPI-anchor remodeling: Potential functions of GPI-anchors in intracellular trafficking and membrane dynamics. Biochim Biophys Acta 1821:1050–1058.

Hansen L, Tawamie H, Murakami Y, Mang Y, ur Rehman S, Buchert R, Schaffer S, Muhammad S, Bak M, Nothen MM, Bennett EP, Maeda Y, Aigner M, Reis A, Kinoshita T, Tommerup N, Baig SM, Abou Jamra R. 2013. Hypomorphic mutations in PGAP2, encoding a GPI-anchor-remodeling protein, cause autosomal-recessive intellectual disability. Am J Hum Genet 92:575–583.

Horn D, Krawitz P, Mannhardt A, Korenke GC, Meinecke P. 2011. Hyperphosphatasia-mental retardation syndrome due to PIGV mutations: Expanded clinical spectrum. Am J Med Genet Part A 155A:1917–1922.

Howard MF, Murakami Y, Pagnamenta AT, Daumer-Haas C, Fischer B, Hecht J, Keays DA, Knight SJ, Kolsch U, Kruger U, Leiz S, Maeda Y, Mitchell D, Mundlos S, Phillips JA 3rd, Robinson PN, Kini U, Taylor JC, Horn D, Kinoshita T, Krawitz PM. 2014. Mutations in PGAP3 impair GPI-anchor maturation, causing a subtype of hyperphosphatasia with mental retardation. Am J Hum Genet 94:278–287.

Johnston JJ, Gropman AL, Sapp JC, Teer JK, Martin JM, Liu CF, Yuan X, Ye Z, Cheng L, Brodsky RA, Biesecker LG. 2012. The phenotype of a germline mutation in PIGA: The gene somatically mutated in paroxysmal nocturnal hemoglobinuria. Am J Hum Genet 90:295–300.

Krawitz PM, Schweiger MR, Rödelsperger C, Marcelis C, Kölsch U, Meisel C, Stephani F, Kinoshita T, Murakami Y, Bauer S, Isau M, Fischer A, Dahl A, Kerick M, Hecht J, Köhler S, Jäger M, Grünhagen J, de Condor BJ, Doelken S, Brunner HG, Meinecke P, Passarge E, Thompson MD, Cole DE, Horn D, Roscioli T, Mundlos S, Robinson PN. 2010. Identity-by-descent filtering of exome sequence data identifies PIGV mutations in hyperphosphatasia mental retardation syndrome. Nat Genet 42:827–829.

Krawitz Peter M, Murakami Y, Hecht J, Krüger J, Holder U, Susan E, Mortier Geert, Delle Chiaie, De Baere E, Thompson Miles D, Roscioli T, Kielbasa S, Kinoshita T, Mundlos S, Robinson Peter N, Horn D. 2012. Mutations in PIGO, a member of the GPI-anchor-synthesis pathway, cause hyperphosphatasia with mental retardation. Am J Hum Genet 91:146–151.

Krawitz PM, Murakami Y, Riess A, Hietala M, Kruger U, Zhu N, Kinoshita T, Mundlos S, Hecht J, Robinson PN, Horn D. 2013. PGAP2 mutations, affecting the GPI-anchor-synthesis pathway, cause hyperphosphatasia with mental retardation syndrome. Am J Hum Genet 92:584–589.

Kruse K, Hanefeld F, Kohlschutter A, Rosskamp R, Gross-Selbeck G. 1988. Hyperphosphatasia with mental retardation. J Pediatr 112:436–439.

Kvarnung M, Nilsson D, Lindstrand A, Korenke GC, Chiang SC, Blennow E, Bergmann M, Stodberg T, Makitie O, Anderlid BM, Bryceson YT, Nordenskjold M, Nordgren A. 2013. A novel intellectual disability syndrome caused by GPI anchor deficiency due to homozygous mutations in PIGT. J Med Genet 50:521–528.

Mabry CC, Bautista A, Kirk RF, Dubilier LD, Braunstein H, Koepke JA. 1970. Familial hyperphosphatase with mental retardation, seizures, and neurologic deficits. J Pediatr 77:74–85.

Maydan G, Noyman I, Har-Zahav A, Neriah ZB, Pasmanik-Chor M, Yeheskel A, Albin-Kaplanski A, Maya I, Magal N, Birk E, Simon AJ, Halevy A, Rechavi G, Shohat M, Straussberg R, Basel-Vanagaite L. 2011. Multiple congenital anomalies-hypotonia-seizures syndrome is caused by a mutation in PIGN. J Med Genet 48:383–389.

McKenna A, Hanna M, Banks E, Sivachenko A, Cibulskis K, Kernytsky A, Garimella K, Altshuler D, Gabriel S, Daly M, DePristo MA. 2010. The Genome Analysis Toolkit: A MapReduce framework for analyzing next-generation DNA sequencing data. Genome Res 20:1297–1303.

Murakami Y, Kanzawa N, Saito K, Krawitz PM, Mundlos S, Robinson PN, Karadimitris A, Maeda Y, Kinoshita T. 2012. Mechanism for release of alkaline phosphatase caused by glycosylphosphatidylinositol deficiency in patients with hyperphosphatasia mental retardation syndrome. J Biol Chem 287:6318–6325.

Nakamura N, Inoue N, Watanabe R, Takahashi M, Takeda J, Stevens VL, Kinoshita T. 1997. Expression cloning of PIG-L, a candidate N-acetylglucosaminyl-phosphatidylinositol deacetylase. J Biol Chem 272:15834–15840.

Nakamura K, Osaka H, Murakami Y, Anzai R, Nishiyama K, Kodera H, Nakashima M, Tsurusaki Y, Miyake N, Kinoshita T, Matsumoto N, Saitsu H. 2014. PIGO mutations in intractable epilepsy and severe developmental delay with mild elevation of alkaline phosphatase levels. Epilepsia 55:e13–17.

Ng Bobby G, Hackmann K, Jones Melanie A, Eroshkin Alexey M, He P, Wiliams R, Bhide S, Cantagrel V, Gleeson Joseph G, Paller Amy S, Schnur Rhonda E, Tinschert S, Zunich J, Hegde Madhuri R, Freeze Hudson H. 2012. Mutations in the glycosylphosphatidylinositol gene PIGL cause CHIME syndrome. Am J Hum Genet 90:685–688.

Ohba C, Okamoto N, Murakami Y, Suzuki Y, Tsurusaki Y, Nakashima M, Miyake N, Tanaka F, Kinoshita T, Matsumoto N, Saitsu H. 2014. PIGN mutations cause congenital anomalies, developmental delay, hypotonia, epilepsy, and progressive cerebellar atrophy. Neurogenetics 15:85–92.

Schnur RE, Greenbaum BH, Heymann WR, Christensen K, Buck AS, Reid CS. 1997. Acute lymphoblastic leukemia in a child with the CHIME neuroectodermal dysplasia syndrome. Am J Med Genet 72:24–29.

Shashi V, Zunich J, Kelly TE, Fryburg JS. 1995. Neuroectodermal (CHIME) syndrome: An additional case with long term follow up of all reported cases. J Med Genet 32:465–469.

Wang K, Li M, Hakonarson H. 2010. ANNOVAR: Functional annotation of genetic variants from high-throughput sequencing data. Nucleic Acids Res 38:e164.

Ware RE, Rosse WF, Howard TA. 1994. Mutations within the Piga gene in patients with paroxysmal nocturnal hemoglobinuria. Blood 83:2418–2422.

Watanabe R, Ohishi K, Maeda Y, Nakamura N, Kinoshita T. 1999. Mammalian PIG-L and its yeast homologue Gpi12p are N-acetylglucosaminylphosphatidylinositol de-N-acetylases essential in glycosylphosphatidylinositol biosynthesis. Biochem J 339:185–192.

CLINICAL REPORT

AMERICAN JOURNAL OF medical genetics PART A

Compound Heterozygous Deletions in Pseudoautosomal Region 1 in an Infant With Mild Manifestations of Langer Mesomelic Dysplasia

Takayoshi Tsuchiya,[1,2] Minoru Shibata,[3] Hironao Numabe,[3,4] Tomoko Jinno,[1] Kazuhiko Nakabayashi,[5] Gen Nishimura,[6] Toshiro Nagai,[2] Tsutomu Ogata,[1,7] and Maki Fukami[1]*

[1]Department of Molecular Endocrinology, National Research Institute for Child Health and Development, Tokyo, Japan

[2]Department of Pediatrics, Dokkyo Medical University Koshigaya Hospital, Koshigaya, Japan

[3]Department of Pediatrics, Kyoto University Hospital, Kyoto, Japan

[4]Graduate School of Humanities and Sciences, Ochanomizu University, Tokyo, Japan

[5]Department of Maternal-Fetal Biology, National Research Institute for Child Health and Development, Tokyo, Japan

[6]Department of Pediatric Imaging, Tokyo Metropolitan Children's Medical Center, Tokyo, Japan

[7]Department of Pediatrics, Hamamatsu University School of Medicine, Hamamatsu, Japan

Manuscript Received: 15 May 2013; Manuscript Accepted: 13 September 2013

Haploinsufficiency of *SHOX* on the short arm pseudoautosomal region (PAR1) leads to Leri–Weill dyschondrosteosis (LWD), and nullizygosity of *SHOX* results in Langer mesomelic dysplasia (LMD). Molecular defects of LWD/LMD include various microdeletions in PAR1 that involve exons and/or the putative upstream or downstream enhancer regions of *SHOX*, as well as several intragenic mutations. Here, we report on a Japanese male infant with mild manifestations of LMD and hitherto unreported microdeletions in PAR1. Clinical analysis revealed mesomelic short stature with various radiological findings indicative of LMD. Molecular analyses identified compound heterozygous deletions, that is, a maternally inherited ~46 kb deletion involving the upstream region and exons 1–5 of *SHOX*, and a paternally inherited ~500 kb deletion started from a position ~300 kb downstream from *SHOX*. In silico analysis revealed that the downstream deletion did not affect the known putative enhancer regions of *SHOX*, although it encompassed several non-coding elements which were well conserved among various species with *SHOX* orthologs. These results provide the possibility of the presence of a novel enhancer for *SHOX* in the genomic region ~300 to ~800 kb downstream of the start codon.

Key words: *SHOX*; langer mesomelic dysplasia; deletion; enhancer

How to Cite this Article:
Tsuchiya T, Shibata M, Numabe H, Jinnno T, Nakabayashi K, Nishimura G, Nagai T, Ogata T, Fukami M. 2013. Compound heterozygous deletions in pseudoautosomal region 1 in an infant with mild manifestations of langer mesomelic dysplasia.
Am J Med Genet Part A 9999:1–6.

INTRODUCTION

SHOX on the short arm pseudoautosomal region (PAR1) is a transcription factor gene exclusively expressed in the developing limbs and pharyngeal arches [Rao et al., 1997; Clement-Jones et al., 2000]. Haploinsufficiency of *SHOX* leads to idiopathic short stature and Leri–Weill dyschondrosteosis (LWD; OMIM #127300), and nullizygosity of *SHOX* results in Langer mesomelic dysplasia (LMD; OMIM #249700) [Rao et al., 1997; Belin et al., 1998; Shears et al., 1998; Zinn et al., 2002]. Previous studies in patients with LWD and LMD have identified several copy-number abnormalities in PAR1 that involved coding exons and/or the putative upstream or downstream enhancer regions, together with multiple point

We declare no potential conflicts of interest relevant to this article.
Grant sponsor: Ministry of Health, Labor and Welfare; Grant sponsor: Ministry of Education, Culture, Sports, Science and Technology; Grant sponsor: National Center for Child Health and Development; Grant sponsor: Takeda Science Foundation; Grant sponsor: Daiichi-Sankyo Foundation of Life Science.

*Correspondence to:
Maki Fukami, Department of Molecular Endocrinology, National Research Institute for Child Health and Development, 157-8535 Tokyo, Japan.
E-mail: fukami-m@ncchd.go.jp

Article first published online in Wiley Online Library (wileyonlinelibrary.com): 00 Month 2013
DOI 10.1002/ajmg.a.36284

mutations in the coding region [Rao et al., 1997; Belin et al., 1998; Shears et al., 1998; Benito-Sanz et al., 2005, 2011, 2012b; Fukami et al., 2005, 2006; Bertorelli et al., 2007; Sabherwal et al., 2007; Chen et al., 2009; Durand et al., 2010]. The putative enhancers of *SHOX* have been mapped to a ~300 kb region ~95 kb upstream, and to a ~30 kb region ~250 kb downstream from the start codon [Benito-Sanz et al., 2005, 2012a,b; Fukami et al., 2006]. The putative downstream enhancer region contains several conserved non-coding elements (CNEs) that exert enhancer activity in the developing chicken limb bud [Sabherwal et al., 2007] and in human osteosarcoma cells [Fukami et al., 2006; Benito-Sanz et al., 2012b]. Since molecular abnormalities have not been detected in a substantial portion of patients with LWD/LMD [Zinn et al., 2002; Fukami et al., 2008; Rosilio et al., 2012], it appears that unknown genetic or environmental factors are also involved in the development of these conditions.

The clinical severity of SHOX abnormalities is highly variable [Binder, 2011]. Relatively severe phenotypes in adult female patients indicate that gonadal estrogens enhance skeletal abnormalities in SHOX abnormalities [Ogata et al., 2001; Binder, 2011]. However, there may be other phenotypic modulators for this condition [Binder et al., 2004]. Here, we report on a male infant with mild LMD phenotype and compound heterozygosity of hitherto unreported microdeletions in PAR1.

CLINICAL REPORT

This Japanese male infant was a dizygotic twin conceived by in vitro fertilization. At 24 weeks gestation, an ultrasound examination delineated short extremities in one fetus and a normal skeletal appearance in the other. At 27 weeks gestation, caesarean section was performed because of bradycardia in both fetuses. At birth, the patient presented with a mesomelic appearance with a body length of 33.5 cm (−1.1 SD), weight of 1,130 g (+0.4 SD), and head circumference of 26.5 cm (+1.0 SD). His twin brother was normally proportioned with body length 35.5 cm (−0.1 SD), weight 854 g (−1.5 SD), and head circumference 25.0 cm (±0 SD). Bone survey of the patient at 2 months of age showed markedly curved radii, hypoplastic ulnas and fibulas, and metaphyseal splaying (Fig. 1A). The patient and his brother received standard medical interventions for prematurity, and were discharged from hospital at 3 months of age.

On his latest visit at 21 months of age, the infant manifested obvious mesomelic short stature with a height of 69.3 cm (−3.9 SD), weight of 8.0 kg (−2.7 SD), and head circumference of 46.6 cm (−1.0 SD; Fig. 1B). His developmental milestones were almost normal. His brother had a proportionate short stature with a height of 74.1 cm (−2.6 SD), weight of 8.5 kg (−2.3 SD), and head circumference of 46.2 cm (−1.3 SD). The mother showed limited movement of the wrist and mesomelic short stature (140 cm, −3.6 SD), while the father was clinically normal and had a normal height (165 cm, −1.0 SD). Radiological examinations were not performed for the parents or brother.

MOLECULAR ANALYSES

This study was approved by the Institutional Review Board Committee at the National Center for Child Health and Development.

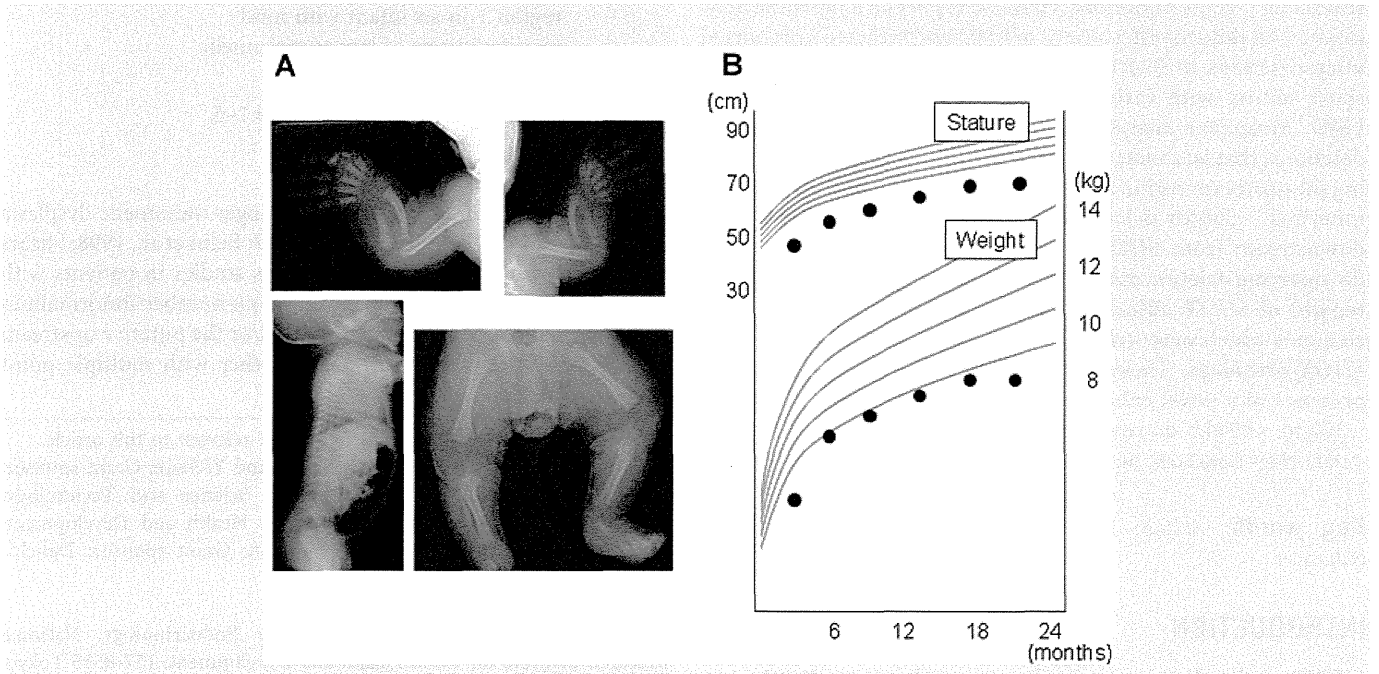

FIG. 1. Clinical findings of the infant. A: X-Ray at 10 weeks of age. Markedly curved radii, hypoplastic ulnas and fibulas, and metaphyseal splaying are shown. B: Growth pattern. Height and weight of the infant are plotted on the longitudinal height and weight standards for Japanese boys (the mean, ±1.0 SD and ±2.0 SD, respectively).

After taking written informed consent from the parents, leukocyte genomic DNA samples were obtained from the infant and parents. First, we performed direct sequencing analysis for *SHOX* by a previously described method [Shears et al., 1998]. No nucleotide alterations in the coding exons were identified in the infant. Next, we performed multiplex ligation-dependent probe amplification (MLPA) using a SALSA MLPA Kit (P018 SHOX-F1, MRC-Holland, Amsterdam, the Netherlands). Two heterozygous deletions in PAR1 were identified in the infant; a deletion involving exons 1–5 of *SHOX*, and a deletion affecting the downstream region of *SHOX* that corresponds to four MLPA probes from 05649-L20176 to 13911-L19678 (Fig. 2). Then, we examined the extent of the deletions by comparative genomic hybridization (CGH) using a custom-built oligo-microarray harboring 26,274 probes for PAR1 and several reference probes for other chromosomal regions (4 × 180 K format, Agilent Technologies, Palo Alto, CA; Fig. 3A). The telomeric deletion included a ~46 kb genomic interval (ChrX: 556,720–603,222; hg 19, Build 37) affecting *SHOX* exons 1–5 and a ~28 kb region at the 5′ side of exon 1. The centromeric deletion encompassed a ~500 kb interval (ChrX: 881,006–1,387,599) and started at a point ~300 kb from the start codon of *SHOX*. In silico analysis using UCSC Genome Browser (http://genome.ucsc.edu/) and rVista 2.0 (http://rvista.dcode.org/) revealed that the deletions did not affect the putative upstream or downstream enhancer regions of *SHOX*, and that the downstream deletion encompassed a gene for cytokine receptor-like factor 2 (*CRLF2*) and several CNEs (Fig. 4). Most of these CNEs were well conserved in fugu, frog, chicken, dog and monkey which preserve orthologs of *SHOX* (*Shox*), as well as in opossum which is likely to preserve *Shox*, and were absent in mouse which lack *Shox* (Ensemble Genome Browser, http://ensembl.org/; Fig. 4). Next, MLPA and CGH were performed on the parental samples. The ~46 and ~500 kb deletions were detected in the mother and father, respectively (Figs. 2 and 3A). Thus, the infant was diagnosed as being compound heterozygous for a maternally inherited ~46 kb deletion on the X chromosome and a paternally inherited ~500 kb deletion on the Y chromosome. The results of MLPA and CGH were confirmed by fluorescence in situ hybridization (FISH). FISH probes for *SHOX* exons 3–5 (probe A) and for a region ~320 kb downstream of *SHOX* (probe B) were generated by PCR using primers 5′-CAGCTCTTCCTCAAATTCTTTCC-3′ and 5′-GTGTCTGTCCCATCTCTGGTATC-3′, and 5′-ATAGTG-CATGGGTATCAGAGGTC-3′ and 5′-GGAAAAAGAGTGGGT-

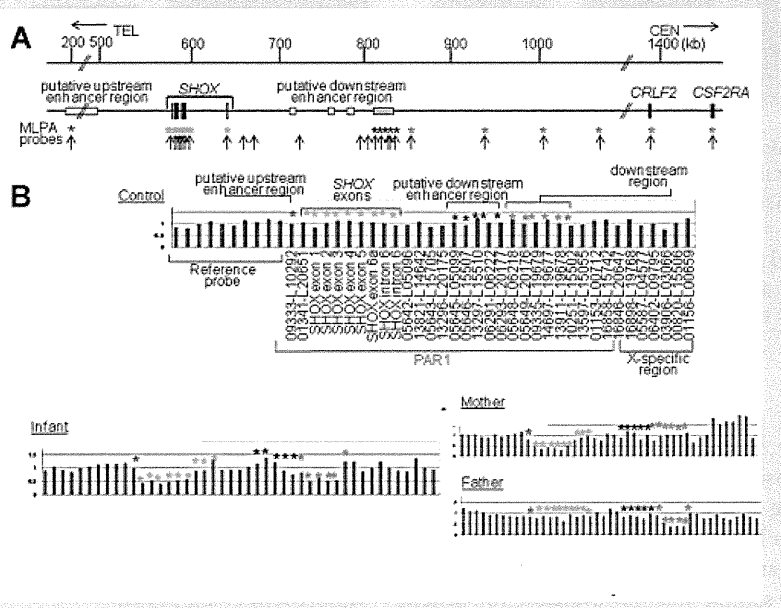

FIG. 2. Multiplex ligation-dependent probe amplification (MLPA) analysis. A: Schematic representation of the short arm pseudoautosomal region (PAR1). The upper horizontal line indicates the physical distance from the Xp/Yp telomere. Genomic positions refer to the Human Genome (hg 19; NCBI Build 37). The black boxes indicate exons of *SHOX*, *CRLF2*, and *CSF2RA* (not all exons are shown). The white box denotes the putative upstream and downstream enhancer regions (elements) of *SHOX* identified in previous studies [Sabherwal et al., 2007; Benito-Sanz et al., 2012a,b]. The gray box indicates putative downstream enhancer elements that exert enhancer activities in the developing chicken limb [Sabherwal et al., 2007]. Vertical arrows indicate genomic positions of MLPA probes; green asterisks indicate probes for *SHOX* exons, blue and black asterisks indicate probes for the putative upstream and downstream enhancer regions respectively, and red asterisks depict probes for the genomic region between the putative downstream enhancer region and *CSF2RA*. TEL, telomere; CEN, centromere. B: Representative results of MLPA. The asterisks indicate the same probes shown in Fig. 2A. The sample data were normalized to a male sample. Decreased peak heights suggest heterozygous deletions. The infant has two deletions; one involving the upstream region and exons 1–5 of *SHOX*, and the other in the downstream region. The mother and father are heterozygous for the deletions.

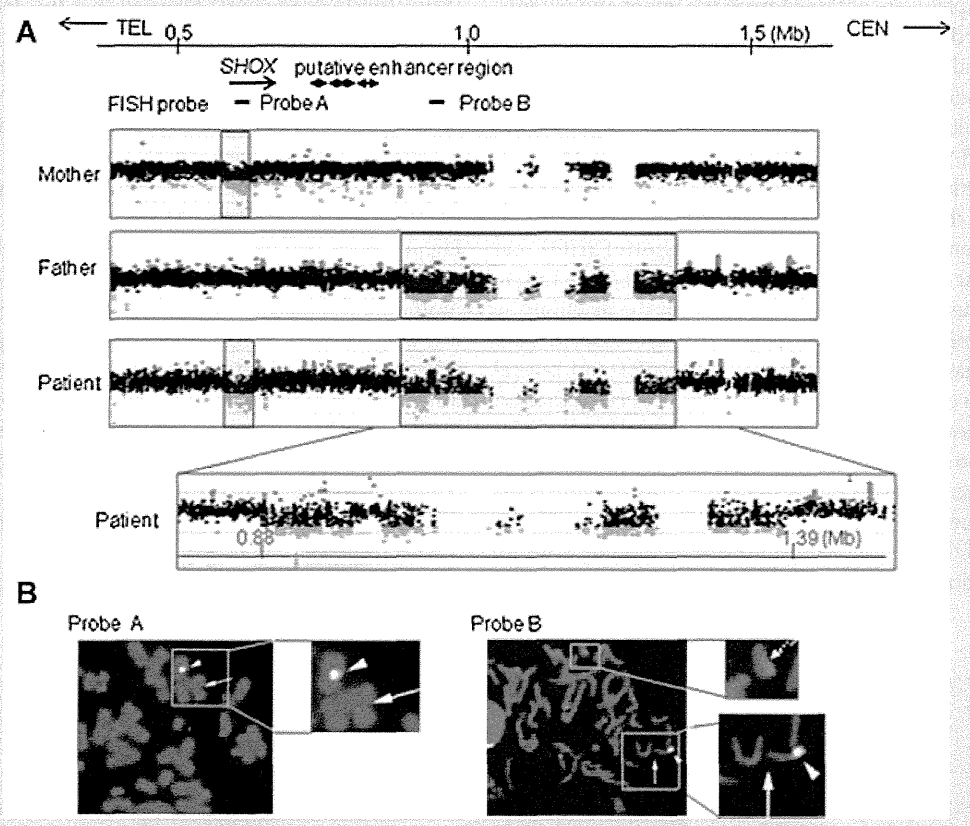

FIG. 3. Comparative genomic hybridization (CGH) and fluorescence in situ hybridization (FISH) analyses. A: CGH analysis in the infant and his parents. The upper horizontal line indicates physical distance from the Xp/Yp telomere. The genomic position of *SHOX*, the putative downstream enhancer elements, and FISH probes are shown. The black, red, and green dots denote signals indicative of the normal, increased (>+0.5), and decreased (<−0.8) copy numbers, respectively. The blue-shaded boxes indicate deleted regions. B: FISH analyses in the infant. Red signals (arrows) indicate probe A for *SHOX* exons 1–3 and probe B for the *SHOX* downstream region, and green signals (arrow heads) depict *DXZ1* control probes on the X chromosome. Probe A detects a signal on the Y chromosome but not on the X chromosome. Probe B detects a signal on the X chromosome but not on the Y chromosome (a dotted arrow).

CAGAACTT-3′, respectively. In the infant, probe A detected only one signal on the Y chromosome and probe B detected only one signal on the X chromosome (Fig. 3B).

We attempted to obtain a DNA sample from the twin brother, because he was predicted to carry the same Y chromosomal deletion as the infant. However, the sample was not available for genetic analysis.

DISCUSSION

We identified compound heterozygous deletions in PAR1 in a male infant. These deletions have not been described previously. The deletion on the X chromosome included most of the coding exons of *SHOX*, and therefore appears to result in complete loss-of-function of the *SHOX* allele. Consistent with this, the mother heterozygous for the same deletion manifested typical clinical features of LWD. In contrast, the deletion on the Y chromosome did not affect exons or the known putative enhancer regions of *SHOX*. Furthermore, this deletion included no genes except *CRLF2*, which has not been implicated in skeletal development [Siracusa et al., 2011]. Clinical examinations of the infant revealed mesomelic short stature and obvious skeletal changes that are more consistent with LMD than with LWD [Fukami et al., 2005; Binder, 2011; Ambrosetti et al., 2013].

Two possible explanations can be made for these results. First, the Y chromosomal deletion in the infant may encompass a hitherto unidentified *cis*-regulatory element of *SHOX*. Recent studies have indicated that several genes such as *SOX9* and *LHX3* have multiple *cis*-acting modules widely distributed around the coding exons [Gordon et al., 2009; Mullen et al., 2012]. Thus, it is possible that coordinated action of multiple regulatory elements is required for adequate *SHOX* expression in the developing limb bud, and that one of such elements is located within the ~500 kb region >300 kb apart from the coding region. Indeed, the Y chromosomal deletion in the infant harbored several CNEs that are well conserved among various species with *SHOX* orthologs.

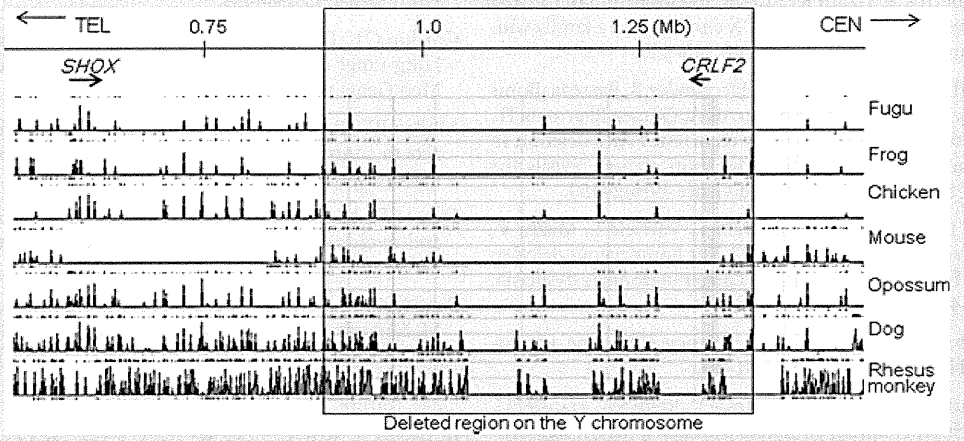

FIG. 4. Conservation analysis in the short arm pseudoautosomal region of the sex chromosomes (PAR1). The deleted region on the Y chromosome (shaded in gray) contains several non-coding elements that are well conserved in species which preserve *SHOX* orthologs (fugu, frog, chicken, dog, and monkey, and possibly opossum as well) and absent in mouse which lacks an *SHOX* ortholog.

One of the CNEs in the deletion may be a distal enhancer of *SHOX/Shox*, because CNEs in the human genome frequently exert enhancer activity [Pennacchio et al., 2006]. In this regard, it is noteworthy that the skeletal features of this infant are milder than those of previously reported patients with *SHOX* nullizygosity [Zinn et al., 2002; Fukami et al., 2005; Ambrosetti et al., 2013]; the infant showed no short stature or rhizomelia at birth. Furthermore, the father with the same Y chromosomal deletion manifested no skeletal abnormalities, and the twin brother with possible Y chromosomal deletion showed only mild proportionate short stature. These results can be explained by assuming that deletions involving only the putative enhancer regions exert a relatively mild effect on skeletal growth compared to mutations/deletions affecting the coding exons. Consistent with this, relatively mild LWD phenotypes have been observed in patients with heterozygous downstream deletions [Rosilio et al., 2012], and mild LMD phenotype has been described in a patient with compound heterozygous deletions for *SHOX* exons and the putative downstream enhancer region [Fukami et al., 2005]. Alternatively, *cis*-regulatory deletions may be associated with broad phenotypic variation compared to exonic deletions/mutations, because Chen et al. [2009] have described profound phenotypes in patients with enhancer deletions.

Second, the phenotype of the infant may be explained as an extremely severe manifestation of LWD. If this is the case, the Y chromosomal deletion would be a functionally neutral copy-number variation. The absence of skeletal changes in the father with the Y chromosomal deletion supports this notion. In this regard, previous studies have indicated that phenotypic severities of *SHOX* haploinsufficiency are variable and likely to be affected by multiple factors [Binder et al., 2004; Binder, 2011]. Thus, some genetic or environmental factors may have enhanced the abnormal skeletal formation of this infant with a maternally derived *SHOX* intragenic deletion.

In summary, we identified hitherto unreported deletions in PAR1 in a Japanese infant with a mild LMD phenotype. Further studies will clarify the presence or absence of a novel downstream enhancer of *SHOX* in the genomic region ~300 to ~800 kb from the start codon.

ACKNOWLEDGMENTS

This work was supported by grants from the following: the Ministry of Health, Labor and Welfare, the Ministry of Education, Culture, Sports, Science and Technology, the National Center for Child Health and Development, the Takeda Science Foundation, and Daiichi-Sankyo Foundation of Life Science.

REFERENCES

Ambrosetti F, Palicelli A, Bulfamante G, Rivasi F. 2013. Langer mesomelic dysplasia in early fetuses: Two cases and a literature review. Fetal Pediatr Pathol [Epub ahead of print].

Belin V, Cusin V, Viot G, Girlich D, Toutain A, Moncla A, Vekemans M, Le Merrer M, Munnich A, Cormier-Daire V. 1998. SHOX mutations in dyschondrosteosis (Leri–Weill syndrome). Nat Genet 19:67–69.

Benito-Sanz S, Thomas NS, Huber C, Gorbenko del Blanco D, Aza-Carmona M, Crolla JA, Maloney V, Rappold G, Argente J, Campos-Barros A, Cormier-Daire V, Heath KE. 2005. A novel class of pseudoautosomal region 1 deletions downstream of SHOX is associated with Leri–Weill dyschondrosteosis. Am J Hum Genet 77:533–544.

Benito-Sanz S, Barroso E, Heine-Suñer D, Hisado-Oliva A, Romanelli V, Rosell J, Aragones A, Caimari M, Argente J, Ross JL, Zinn AR, Gracia R, Lapunzina P, Campos-Barros A, Heath KE. 2011. Clinical and molecular evaluation of SHOX/PAR1 duplications in Leri–Weill dyschondrosteosis (LWD) and idiopathic short stature (ISS). J Clin Endocrinol Metab 96: E404–E412.

Benito-Sanz S, Aza-Carmona M, Rodríguez-Estevez A, Rica-Etxebarria I, Gracia R, Campos-Barros A, Heath KE. 2012a. Identification of the first PAR1 deletion encompassing upsream SHOX enhancers in a family with idiopathic short stature. Eur J Hum Genet 20:125–127.

Benito-Sanz S, Royo JL, Barroso E, Paumard-Hernández B, Barreda-Bonis AC, Liu P, Gracia R, Lupski JR, Campos-Barros Á, Gómez-Skarmeta JL, Heath KE. 2012b. Identification of the first recurrent PAR1 deletion in Léri–Weill dyschondrosteosis and idiopathic short stature reveals the presence of a novel SHOX enhancer. J Med Genet 49:442–450.

Bertorelli R, Capone L, Ambrosetti F, Garavelli L, Varriale L, Mazza V, Stanghellini I, Percesepe A, Forabosco A. 2007. The homozygous deletion of the 3′ enhancer of the SHOX gene causes Langer mesomelic dysplasia. Clin Genet 72:490–491.

Binder G. 2011. Short stature due to SHOX deficiency: Genotype, phenotype, and therapy. Horm Res Paediatr 75:81–89.

Binder G, Renz A, Martinez A, Keselman A, Hesse V, Riedl SW, Häusler G, Fricke-Otto S, Frisch H, Heinrich JJ, Ranke MB. 2004. SHOX haploinsufficiency and Leri–Weill dyschondrosteosis: Prevalence and growth failure in relation to mutation, sex, and degree of wrist deformity. J Clin Endocrinol Metab 89:4403–4408.

Chen J, Wildhardt G, Zhong Z, Röth R, Weiss B, Steinberger D, Decker J, Blum WF, Rappold G. 2009. Enhancer deletions of the SHOX gene as a frequent cause of short stature: The essential role of a 250 kb downstream regulatory domain. J Med Genet 46:834–839.

Clement-Jones M, Schiller S, Rao E, Blaschke RJ, Zuniga A, Zeller R, Robson SC, Binder G, Glass I, Strachan T, Lindsay S, Rappold GA. 2000. The short stature homeobox gene SHOX is involved in skeletal abnormalities in Turner syndrome. Hum Mol Genet 9:695–702.

Durand C, Bangs F, Signolet J, Decker E, Tickle C, Rappold G. 2010. Enhancer elements upstream of the SHOX gene are active in the developing limb. Eur J Hum Genet 18:527–532.

Fukami M, Okuyama T, Yamamori S, Nishimura G, Ogata T. 2005. Microdeletion in the SHOX 3′ region associated with skeletal phenotypes of Langer mesomelic dysplasia in a 45,X/46,X,r(X) infant and Leri–Weill dyschondrosteosis in her 46, XX mother: Implication for the SHOX enhancer. Am J Med Genet Part A 137A:72–76.

Fukami M, Kato F, Tajima T, Yokoya S, Ogata T. 2006. Transactivation function of an approximately 800-bp evolutionarily conserved sequence at the SHOX 3′ region: Implication for the downstream enhancer. Am J Hum Genet 78:167–170.

Fukami M, Dateki S, Kato F, Hasegawa Y, Mochizuki H, Horikawa R, Ogata T. 2008. Identification and characterization of cryptic SHOX intragenic deletions in three Japanese patients with Léri–Weill dyschondrosteosis. J Hum Genet 53:454–459.

Gordon CT, Tan TY, Benko S, Fitzpatrick D, Lyonnet S, Farlie PG. 2009. Long-range regulation at the SOX9 locus in development and disease. J Med Genet 46:649–656.

Mullen RD, Park S, Rhodes SJ. 2012. A distal modular enhancer complex acts to control pituitary- and nervous system-specific expression of the LHX3 regulatory gene. Mol Endocrinol 26:308–319.

Ogata T, Matsuo N, Nishimura G. 2001. SHOX haploinsufficiency and overdosage: Impact of gonadal function status. J Med Genet 38: 1–6.

Pennacchio LA, Ahituv N, Moses AM, Prabhakar S, Nobrega MA, Shoukry M, Minovitsky S, Dubchak I, Holt A, Lewis KD, Plajzer-Frick I, Akiyama J, De Val S, Afzal V, Black BL, Couronne O, Eisen MB, Visel A, Rubin EM. 2006. In vivo enhancer analysis of human conserved non-coding sequences. Nature 23:499–502.

Rao E, Weiss B, Fukami M, Rump A, Niesler B, Mertz A, Muroya K, Binder G, Kirsch S, Winkelmann M, Nordsiek G, Heinrich U, Breuning MH, Ranke MB, Rosenthal A, Ogata T, Rappold GA. 1997. Pseudoautosomal deletions encompassing a novel homeobox gene cause growth failure inidiopathic short stature and Turner syndrome. Nat Genet 16:54–63.

Rosilio M, Huber-Lequesne C, Sapin H, Carel JC, Blum WF, Cormier-Daire V. 2012. Genotypes and phenotypes of children with SHOX deficiency in France. J Clin Endocrinol Metab 97:E1257–E1265.

Sabherwal N, Bangs F, Röth R, Weiss B, Jants K, Tiecke E, Hinkel GK, Spaich C, Hauffa BP, van der Kamp H, Kapeller J, Tickle C, Rappold G. 2007. Long-range conserved non-coding SHOX sequences regulate expression in developing chicken limb and are associated with short stature phenotypes in human patients. Hum Mol Genet 16:210–222.

Shears DJ, Vassal HJ, Goodman FR, Palmer RW, Reardon W, Superti-Furga A, Scambler PJ, Winter RM. 1998. Mutation and deletion of the pseudoautosomal gene SHOX cause Leri–Weill dyschondrosteosis. Nat Genet 19:70–73.

Siracusa MC, Saenz SA, Hill DA, Kim BS, Headley MB, Doering TA, Wherry EJ, Jessup HK, Siegel LA, Kambayashi T, Dudek EC, Kubo M, Cianferoni A, Spergel JM, Ziegler SF, Comeau MR, Artis D. 2011. TSLP promotes interleukin-3-independent basophil haematopoiesis and type 2 inflammation. Nature 14:229–233.

Zinn AR, Wei F, Zhang L, Elder FF, Scott CI Jr, Marttila P, Ross JL. 2002. Complete SHOX deficiency causes Langer mesomelic dysplasia. Am J Med Genet 110:158–163.

Clinical Endocrinology (2013) doi: 10.1111/cen.12379

ORIGINAL ARTICLE

IMAGe syndrome: clinical and genetic implications based on investigations in three Japanese patients

Fumiko Kato*, Takashi Hamajima†, Tomonobu Hasegawa‡, Naoko Amano‡, Reiko Horikawa§, Gen Nishimura¶, Shinichi Nakashima*, Tomoko Fuke**, Shinichirou Sano**, Maki Fukami** and Tsutomu Ogata*

*Department of Pediatrics, Hamamatsu University School of Medicine, Hamamatsu, †Division of Endocrinology and Metabolism, Aichi Children's Health and Medical Center, Obu, ‡Department of Pediatrics, Keio University School of Medicine, §Division of Endocrinology and Metabolism, National Center for Child Health and Development, Tokyo, ¶Department of Radiology, Tokyo Metropolitan Children's Medical Center, Fuchu, and **Department of Molecular Endocrinology, National Research Institute for Child Health and Development, Tokyo, Japan

Summary

Objective Arboleda *et al.* have recently shown that IMAGe (intra-uterine growth restriction, metaphyseal dysplasia, adrenal hypoplasia congenita and genital abnormalities) syndrome is caused by gain-of-function mutations of maternally expressed gene *CDKN1C* on chromosome 11p15.5. However, there is no other report describing clinical findings in patients with molecularly studied IMAGe syndrome. Here, we report clinical and molecular findings in Japanese patients.

Patients We studied a 46,XX patient aged 8·5 years (case 1) and two 46,XY patients aged 16·5 and 15·0 years (cases 2 and 3).

Results Clinical studies revealed not only IMAGe syndrome-compatible phenotypes in cases 1–3, but also hitherto undescribed findings including relative macrocephaly and apparently normal pituitary-gonadal endocrine function in cases 1–3, familial glucocorticoid deficiency (FGD)-like adrenal phenotype and the history of oligohydramnios in case 2, and arachnodactyly in case 3. Sequence analysis of *CDKN1C*, pyrosequencing-based methylation analysis of KvDMR1 and high-density oligonucleotide array comparative genome hybridization analysis for chromosome 11p15.5 were performed, showing an identical *de novo* and maternally inherited *CDKN1C* gain-of-function mutation (p.Asp274Asn) in cases 1 and 2, respectively, and no demonstrable abnormality in case 3.

Conclusions The results of cases 1 and 2 with *CDKN1C* mutation would argue the following: [1] relative macrocephaly is consistent with maternal expression of *CDKN1C* in most tissues and biparental expression of *CDKN1C* in the foetal brain; [2] FGD-like phenotype can result from *CDKN1C* mutation; and [3] genital abnormalities may primarily be ascribed to placental dysfunction. Furthermore, lack of *CDKN1C* mutation in case 3 implies genetic heterogeneity in IMAGe syndrome.

(Received 1 October 2013; returned for revision 24 November 2013; finally revised 26 November 2013; accepted 29 November 2013)

Introduction

IMAGe syndrome is a multisystem developmental disorder named by the acronym of intra-uterine growth restriction (IUGR), metaphyseal dysplasia and adrenal hypoplasia congenita common to both 46,XY and 46,XX patients, and genital abnormalities specific to 46,XY patients.[1] In addition to these salient clinical features, hypercalciuria has been reported frequently in IMAGe syndrome.[1,2] This condition occurs not only as a sporadic form but also as a familial form.[1–3] Furthermore, transmission analysis in a large pedigree has revealed an absolute maternal inheritance of this condition, indicating the relevance of a maternally expressed gene to the development of IMAGe syndrome.[3]

Subsequently, Arboleda *et al.*[4] have mapped the causative gene to a ~17·2-Mb region on chromosome 11 by an identity-by-descent analysis in this large pedigree and performed targeted exon array capture and high-throughput genomic sequencing for this region in the affected family members and in other sporadic patients. Consequently, they have identified five different missense mutations in the maternally expressed gene *CDKN1C* (cyclin-dependent kinase inhibitor 1C) that resides on the imprinting control region 2 (ICR2) domain at chromosome 11p15.5 and encodes a negative regulator for cell proliferation.[4–6] Notably, all the missense mutations are clustered within a specific segment of PCNA-binding domain, and functional studies have implicated that these mutations have gain-of-function effects.[4] Thus, IMAGe syndrome appears to constitute a mirror image of Beckwith–Wiedemann syndrome (BWS) in terms of the

Correspondence: Dr. Tsutomu Ogata, Department of Pediatrics, Hamamatsu University School of Medicine, 1-20-1 Handayama, Higashi-ku, Hamamatsu 431-3192, Japan. Tel./Fax: +81 53 435 2310; E-mail: tomogata@hama-med.ac.jp

CDKN1C function, because multiple *CDKN1C* loss-of-function mutations have been identified in BWS with no mutation shared in common by IMAGe syndrome and BWS.[4,5]

However, several matters remain to be clarified in IMAGe syndrome, including phenotypic spectrum and underlying mechanism(s) for the development of each phenotype in *CDKN1C*-mutation-positive patients, and the presence or absence of genetic heterogeneity. Here, we report clinical and molecular findings in three patients with IMAGe syndrome and discuss these unresolved matters.

Patients and methods

Patients

We studied one previously described 46,XX patient (case 1)[7] and two hitherto unreported 46,XY patients (cases 2 and 3). In cases 1–3, no pathologic mutations were identified in the coding exons and their splice cites of *NR5A1* (*SF1*) and *NR0B1* (*DAX1*) relevant to adrenal hypoplasia,[8] and *MC2R*, *MRAP*, *STAR* and *NNT* involved in familial glucocorticoid deficiency (FGD).[9]

Ethical approval and samples

This study was approved by the Institutional Review Board Committee at Hamamatsu University School of Medicine. Molecular studies were performed using leucocyte genomic DNA samples of cases 1–3 and the parents of cases 1 and 2, after obtaining written informed consent.

Sequence analysis of CDKN1C

The coding exons 1 and 2 and their flanking splice sites were amplified by polymerase chain reaction (PCR) (Fig. 1a), using primers shown in Table S1. Subsequently, the PCR products were subjected to direct sequencing from both directions on ABI 3130 autosequencer (Life Technologies, Carlsbad, CA, USA). In this regard, if a nucleotide variation were present within the primer-binding site(s), this may cause a false-negative finding because of amplification failure of a mutation-positive allele. Thus, PNCA-binding domain was examined with different primer sets. To confirm a heterozygous mutation, the corresponding PCR products were subcloned with TOPO TA Cloning Kit (Life Technologies), and normal and mutant alleles were sequenced separately.

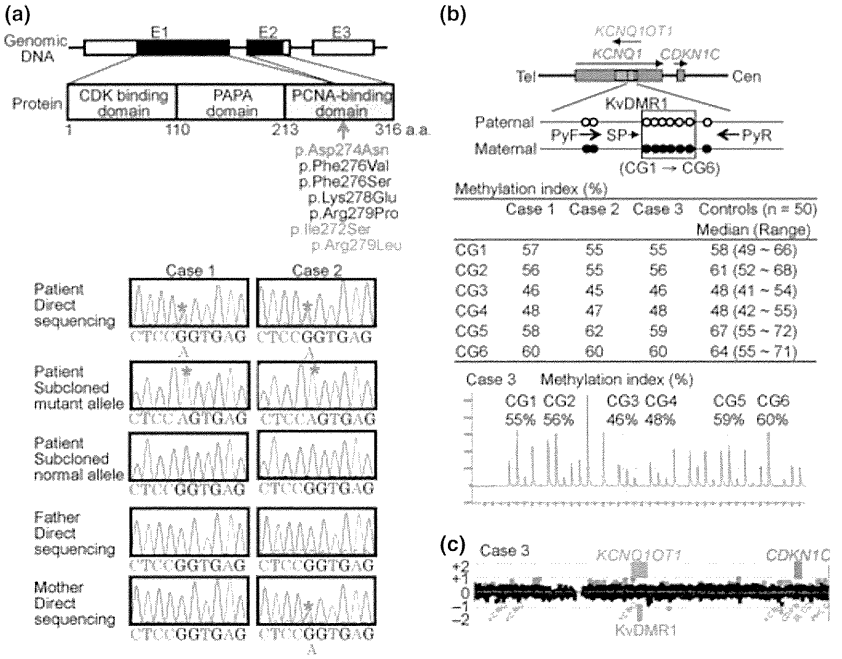

Fig. 1 Summary of molecular studies. (a) Sequence analysis of *CDKN1C*. *CDKN1C* consists of three exons (E1–E3), and the black and white boxes denote the coding regions and the untranslated regions, respectively. CDKN1C protein is composed of 316 amino acids and contains CDK binding domain, PAPA domain and PCNA-binding domain. The p.Asp274Asn mutation found in this study and the previous study[4] is shown in red. The four mutations written in black have also been identified in IMAGe syndrome.[4] The pIle272Ser mutation written in green has been detected in atypical IMAGe syndrome lacking skeletal lesion,[22] and the pArg279Leu mutation written in blue has been found in SRS.[24] Electrochromatograms denote a *de novo* p.Asp274Asn mutation in case 1 and a maternally inherited p.Asp274Asn mutation in case 2. (b) Methylation analysis of KvDMR1 at the ICR2 domain. The cytosine residues at the CpG dinucleotides are unmethylated after paternal transmission (open circles) and methylated after maternal transmission (filled circles). *KCNQ1OT1* is a paternally expressed gene, and *KCNQ1* and *CDKN1C* are maternally expressed genes. The six CpG dinucleotides (CG1→CG6) examined by pyrosequencing are highlighted with a yellow rectangle, and the positions of PyF & PyR primers and SP are shown by thick arrows and a thin arrow, respectively. A pyrogram of case 3 is shown. (c) Array CGH analysis for chromosome 11p15.5 encompassing the ICR2 domain in case 3. A region encompassing KvDMR1 and *CDKN1C* is shown. Black, red and green dots denote signals indicative of the normal, the increased (>+0·5) and the decreased (<−1·0) copy numbers, respectively. Although several red and green signals are seen, there is no portion associated with ≥3 consecutive red or green signals.

Methylation analysis of KvDMR1 and array CGH analysis for chromosome 11p15.5

Increased expression of *CDKN1C*, as well as gain-of-function mutations of *CDKN1C*, may lead to IMAGe syndrome. Such increased *CDKN1C* expression would occur in association with hypermethylated KvDMR1 (differentially methylated region 1) at the ICR2 domain, because *CDKN1C* is expressed when the *cis*-situated KvDMR1 is methylated as observed after maternal transmission and is repressed when the *cis*-situated KvDMR1 is unmethylated as observed after paternal transmission.[5] Thus, we performed pyrosequencing analysis for six CpG dinucleotides (CG1–CG6) within KvDMR1, using bisulphite-treated leucocyte genomic DNA samples (Fig. 1b). In brief, a 155-bp region was PCR-amplified with a primer set (PyF and PyR) for both methylated and unmethylated clones, and a sequence primer (SP) was hybridized to single-stranded PCR products (for PyF, PyR and SP sequences, see Table S1). Subsequently, methylation index (MI, the ratio of methylated clones) was obtained for each CpG dinucleotide, using PyroMark Q24 (Qiagen, Hilden, Germany). To define the reference ranges of MIs, 50 control subjects were similarly studied with permission.

Increased *CDKN1C* expression may also result from a copy number gain of the maternally inherited ICR2 domain. Thus, we performed high-density array CGH (comparative genomic hybridization) using a custom-build 33 088 oligonucleotide probes for chromosome 11p15.5 encompassing the ICR2 domain, together with ~10 000 reference probes for other chromosomal regions (Agilent Technologies, Santa Clara, CA, USA). The procedure was carried out as described in the manufacturer's instructions.

Results

Clinical findings

Detailed clinical findings are shown in Table 1. Cases 1–3 exhibited characteristic faces with frontal bossing, flat nasal root, low set ears and mild micrognathia, as well as short limbs. They had IUGR and postnatal growth failure. Notably, while birth and present length/height and weight were severely compromised, birth and present occipitofrontal circumference (OFC) were relatively well preserved. Radiological examinations revealed generalized osteopenia, delayed bone maturation and metaphyseal dysplasia with vertical sclerotic striations of the knee in cases 1–3, slender bones in cases 1 and 2, scoliosis in cases 2 and 3, arachnodactyly in case 3 and broad distal phalanx of the thumbs and great toes in case 2 (Fig. 2). Cases 1 and 3 experienced adrenal crisis in early infancy and received glucocorticoid and mineralocorticoid supplementation therapy since infancy. Case 2 had transient neonatal hyponatremia and several episodes of hypoglycaemia without electrolyte abnormality in childhood and was found to have hypoglycaemia and hyponatremia without hyperkalemia when he had severe viral gastroenteritis at 15·5 years of age. Thus, an adrenocorticotropic hormone stimulation test was performed after recovery from gastroenteritis, revealing poor cortisol response. Thereafter, he was placed on glucocorticoid supplementation therapy. As serum electrolytes were normal, mineralocorticoid supplementation therapy was not initiated. Genital abnormalities included cryptorchidism and small testes in cases 2 and 3, and hypospadias in case 3. However, pituitary-gonadal endocrine function was apparently normal in cases 1–3. Urine calcium secretion was borderline high or increased in cases 1–3, although serum calcium and calcium homeostasis-related factors were normal. In addition, feeding difficulties during infancy were observed in cases 1 and 2, but not in case 3, and oligohydramnios was noticed during the pregnancy of case 2. There was no body asymmetry in cases 1–3. Thus, clinical studies in cases 1–3 revealed not only IMAGe syndrome-compatible phenotypes, but also hitherto undescribed clinical finding (Table 2).

Sequence analysis of CDKN1C

A heterozygous identical missense mutation (c.820G>A, p.Asp274Asn) was identified in cases 1 and 2 (Fig. 1a). This mutation occurred as a *de novo* event in case 1 and was inherited from the phenotypically normal mother in case 2. No demonstrable mutation was identified in case 3.

Methylation analysis of KvDMR1 and array CGH analysis for chromosome 11p15.5

The MIs for CG1–CG6 were invariably within the normal range in cases 1–3 (Fig. 1b), and no discernible copy number alteration was identified in cases 1–3 (Fig. 1c). The results excluded maternal uniparental disomy involving KvDMR1, hypermethylation (epimutation) of the paternally inherited KvDMR1 and submicroscopic duplication involving the maternally derived ICR2 domain, as well as submicroscopic deletion affecting the paternally derived ICR2 domain.

Discussion

CDKN1C mutations in IMAGe syndrome

We identified a heterozygous *CDKN1C* missense mutation (Asp274Asn) in cases 1 and 2. This mutation has previously been detected in a patient with IMAGe syndrome.[4] Furthermore, *de novo* occurrence of the mutation in case 1 argues for the mutation being pathologic, and maternal transmission of the mutation in case 2 is consistent with *CDKN1C* being a maternally expressed gene. Thus, our results provide further evidence for specific missense mutations of *CDKN1C* being responsible for the development of IMAGe syndrome.

Clinical features in CDKN1C*-mutation-positive cases 1 and 2*

Several matters are noteworthy with regard to clinical findings in *CDKN1C*-mutation-positive cases 1 and 2. First, although

Table 1. Clinical findings of cases 1–3

	Case 1*	Case 2	Case 3
Karyotype	46,XX	46,XY	46,XY
Present age (year)	8·5	16·5	15·0
Characteristic face	Yes	Yes	Yes
Pre- and postnatal growth			
Gestational age (week)	35	37	38
Birth length (cm) (SDS)	37·0 (−3·5)	40·0 (−4·0)	41·0 (−4·3)
Birth weight (kg) (SDS)	1·34 (−2·9)	2·03 (−3·5)	1·71 (−3·4)
Birth OFC (cm) (SDS)	30·7 (−0·3)	32·0 (−0·9)	33·0 (−0·1)
Birth BMI (kg/m^2) (percentile)	9·8 (<3)	12·7 (50)	10·1 (<3)
BMI (kg/m^2) at 2 years of age (SDS)	14·2 (−1·8)	13·0 (−3·4)	Unknown
Present height (cm) (SDS)	92·8 (−6·2)	124·7 (−7·8)	135·2 (−5·1)
Present weight (kg) (SDS)	16·0 (−1·9)	25·4 (−3·5)	30·4 (−2·6)
Present OFC (cm) (SDS)	52·0 (−0·2)	53·0 (−2·5)	Unknown
Present BMI (kg/m^2) (SDS)	18·6 (+1·6)	16·3 (−2·6)	16·6 (−1·7)
Skeletal abnormality			
Examined age (year)	5·5	16·5	15·0
Generalized osteopenia	Yes	Yes	Yes
Delayed maturation	Yes	Yes	Yes
Metaphyseal dysplasia	Yes	Yes	Yes
Slender bones	Yes	Yes	No
Scoliosis	No	Yes	Yes
Arachnodactyly	No	No	Yes
Broad thumbs & big toes	No	Yes	No
Adrenal dysfunction			
Examined age (year) before therapy	0·1 (39 days)	15·5	0·5 (6 months)
MRI/CT	Undetectable	Undetectable	Undetectable
ACTH (pg/ml)	9010 [19·9 ± 8·8]	427 [22·9 ± 6·2]	>1000 [22·9 ± 6·2]
Cortisol (μg/dl)	8·4 [8·3 ± 3·4]	6·9 [9·5 ± 2·9]	<1·0 [9·5 ± 2·9]
After ACTH stimulation†	N.E.	9·4 [> 20]	<1·0 [> 20]
Plasma renin activity (ng/ml/h)	N.E.	6·0 [1·0 ± 0·1]	>25 [1·01 ± 0·14]
Active renin concentration (pg/ml)	21 400 [2·5–21·4]	N.E.	N.E.
Aldosterone (ng/dl)	6·9 [9·7 ± 4·5]	5·2 [8·5 ± 1·4]	4·1 [7·4 ± 2·2]
Na (mEq/l)	122 [135–145]	141 (127‡) [135–145]	126 [135–145]
K (mEq/l)	8·0 [3·7–4·8]	4·2 (4·0‡) [3·7–4·8]	6·5 [3·7–4·8]
Cl (mEq/l)	86 [98–108]	103 (98‡) [98–108]	89 [98–108]
Glucocorticoid therapy	Yes (since 2 months)	Yes (since 15·5 years)	Yes (since 6 months)
Mineralocorticoid therapy	Yes (since 2 months)	No	Yes (since 6 months)
Genital abnormality			
Examined age (year)	8·5	16·5	15·0
Hypospadias	–	No	Yes (operated at 2 years)
Cryptorchidism	–	Yes (B) (operated at 2 years)	Yes (operated at 2 years)
Micropenis	–	No	No
Testis size (R & L) (ml)	–	5 & 8 [13–20]	4 & 10 [11–20]
Pubic hair (Tanner stage)	1 [10·0 ± 1·4 years]§	4 [14·9 ± 0·9 years]¶	4 [14·9 ± 0·9 years]¶
LH (mIU/ml)	<0·1 [<0·1–1·3]	3·9 [0·2–7·8]	4·8 [0·2–7·8]
After GnRH-stimulation**	3·5 [1·6–4·8]	N.E.	N.E.
FSH (mIU/ml)	0·7 [<0·1–5·4]	4·2 [0·3–18·4]	17·6 [0·3–18·4]
After GnRH-stimulation**	12·0 [10·7–38·1]	N.E.	N.E.
Testosterone (ng/ml)	–	4·3 [1·7–8·7]	3·7 [1·7–8·7]
Calcium metabolism			
Examined age (year)	8·5	16·5	15·0
Calcium (mg/dl)	9·7 [8·8–10·5]	9·2 [8·9–10·6]	9·8 [8·9–10·6]
Inorganic phosphate (mg/dl)	3·9 [3·7–5·6]	4·6 [3·1–5·0]	3·8 [3·2–5·1]
Alkaline phosphatase (IU/l)	458 [343–917]	623 [225–680]	309 [225–680]
Intact PTH (pg/ml)	23 [10–65]	43 [10–65]	28 [10–65]
PTHrP (pmol/l)	N.E.	<1·1 [<1·1]	N.E.

(continued)

Clinical Endocrinology (2013), **0**, 1–8

Table 1. (continued)

	Case 1*	Case 2	Case 3
$1,25(OH)_2$ vitamin D (pg/ml)	50 [13–79]	67 [13–79]	50 [13–79]
Urine calcium/creatinine ratio (mg/mg)	0·82 [<0·25]	0·24 [<0·25]	0·44 [<0·25]
%TRP	92 [80–96]	95 [80–96]	94 [80–96]
Others	Feeding difficulties	Feeding difficulties Oligohydramnios	

SDS, standard deviation score; OFC, occipitofrontal circumference; BMI, body mass index; MRI, magnetic resonance imaging; CT, computed tomography; ACTH, adrenocorticotropic hormone; R, right; L, left; LH, luteinizing hormone; FSH, follicle-stimulating hormone; GnRH, gonadotropin-releasing hormone; PTH, parathyroid hormone; PTHrP, PTH-related protein; TRP, tubular reabsorption of phosphate; N.E., not examined; and B, bilateral.
Biochemical values indicate basal blood values, except for those specifically defined.
Birth and present length/height, weight, OFC and BMI have been assessed by sex- and gestational- or age-matched Japanese reference data reported in the literature[26,27] and in the Ministry of Health, Labor, and Welfare Database (http://www.e-stat.go.jp/SG1/estat/GL02020101.do).
The values in brackets represent age- and sex-matched reference values in Japanese children.[28]
The conversion factor to the SI unit: 0·220 for ACTH (pmol/l), 27·6 for cortisol (nmol/l), 0·028 for aldosterone (nmol/l), 3·46 for testosterone (nmol/l), 0·25 for calcium (nmol/l), 0·323 for inorganic phosphate (nmol/l), 0·106 for intact PTH (pmol/l), 2·40 for $1,25(OH)_2$ vitamin D (pmol/l) and 1·0 for plasma renin activity (μg/l/h), active renin concentration (ng/l), Na (nmol/l), K (nmol/l), Cl (nmol/l), LH (IU/l), FSH (IU/l), alkaline phosphatase (IU/l) and PTHrP (pmol/l).
*Clinical findings before 3 years of age have been reported previously.[7]
†ACTH 0·25 mg bolus i.v.; blood sampling at 60 min.
‡Electrolyte values at the time of severe gastroenteritis; other biochemical data in reference to adrenal dysfunction were obtained after recovery from gastroenteritis and before glucocorticoid supplementation therapy.
§Reference age for Tanner stage 2 breast development in Japanese girls.[29]
¶Reference age for Tanner stage 4 pubic hair development in Japanese boys.[29]
**GnRH 100 μg/m^2 bolus i.v.; blood sampling at 0, 30, 60, 90, and 120 min.

Table 2. Summary of clinical features of cases 1–3

	Case 1	Case 2	Case 3
CDKN1C mutation	Yes	Yes	No
Previously reported IMAGe syndrome-compatible phenotype			
IUGR	Yes	Yes	Yes
Metaphyseal dysplasia	Yes	Yes	Yes
Adrenal hypoplasia	Yes*	Yes*	Yes*
Genital abnormality	(Female)	Yes	Yes
Hypercalciura†	Yes	No	Yes
Hitherto undescribed findings			
Body habitus	Relative macrocephaly	Relative macrocephaly	Relative macrocephaly
Skeletal			Arachnodactyly Lack of slender bones
Adrenal		FGD-like phenotype with no obvious mineralocorticoid deficiency	
Genital	Apparently normal pituitary-gonadal endocrine function	Apparently normal pituitary-gonadal endocrine function	Apparently normal pituitary-gonadal endocrine function
Others	Feeding difficulties	Feeding difficulties Oligohydramnios	

IUGR, intrauterine growth retardation; and FGD, familial glucocorticoid deficiency.
*Undetectable on magnetic resonance imaging and/or computed tomography.
†Frequent but not invariable feature.

pre- and postnatal body growth was severely impaired, pre- and postnatal OFC was relatively well preserved. In this regard, while *CDKN1C* is preferentially expressed from the maternal allele in most tissues, it is biparentally expressed at least in the foetal brain.[10] This expression pattern would be relevant to the relative macrocephaly in IMAGe syndrome. Notably, the combination of severely compromised body growth and well-preserved OFC is also characteristic of Silver–Russell syndrome (SRS) resulting

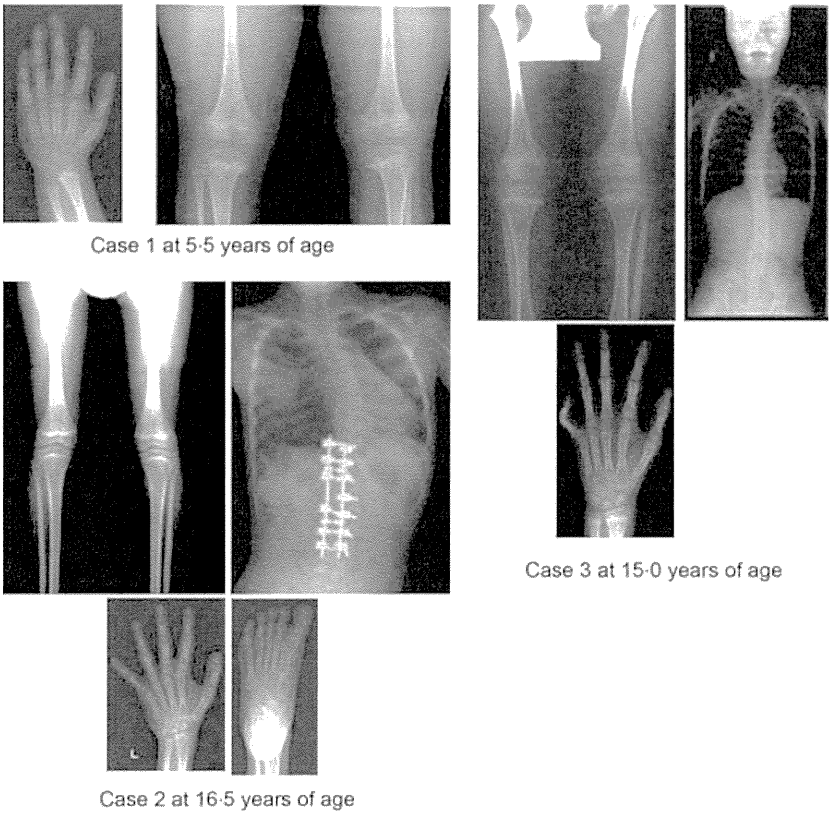

Fig. 2 Representative skeletal roentgenograms in cases 1–3.

from *H19*-DMR hypomethylation (epimutation),[11] and this is primarily consistent with paternal expression of the growth-promoting gene *IGF2* in the body and biparental expression of *IGF2* in the brain.[12] Thus, loss-of-imprinting in the brain tissue appears to underlie relative macrocephaly in both IMAGe syndrome and SRS.

Second, skeletal abnormalities including metaphyseal dysplasia were identified in cases 1 and 2. In this regard, skeletal phenotype of mice lacking *Cdkn1c* is grossly opposite of parathyroid hormone-related protein (PTHrP)-null phenotype,[13,14] and PTHrP permits skeletal development at least in part by suppressing *Cdkn1c* expression.[15] Thus, while serum calcium and calcium homeostasis-related factors were normal in cases 1 and 2, dysregulated PTHrP and/or PTH/PTHrP receptor signalling might be relevant to skeletal abnormalities in patients with gain-of-function mutations of *CDKN1C*. In addition, such a possible signalling defect might also be relevant to the frequent occurrence of hypercalciuria in IMAGe syndrome.

Third, adrenal dysfunction was mild in case 2, while case 1 experienced adrenal crisis in infancy as previously reported in patients with *CDKN1C* mutations.[1,3,4] Indeed, adrenal phenotype of case 2 is similar to that of patients with FGD rather than adrenal hypoplasia.[8,9] Our results therefore would expand the clinical spectrum of adrenal dysfunction in patients with *CDKN1C* mutations. For adrenal dysfunction, cortisol and aldosterone values remained within the normal range at the time of adrenal crisis in case 1 (Table 1). However, as adrenocorticotropic hormone and active renin concentrations were markedly increased, the overall results would be consistent with primary hypoadrenalism, as has been described previously.[16] This notion would also apply to the adrenal dysfunction in case 3 who had apparently normal aldosterone value and markedly increased plasma renin activity at the time of adrenal crisis.

Lastly, although male case 2 had bilateral cryptorchidism and small testes, pituitary-gonadal endocrine function was apparently normal as was secondary sexual development. Previously reported patients with *CDKN1C* mutations, as well as those who have not been examined for *CDKN1C* mutations, also have undermasculinized external genitalia in the presence of apparently normal endocrine function and pubertal development.[1–4,17,18] Notably, an episode of oligohydramnios was found in case 2 and has also been described in a 46,XY IMAGe syndrome patient with cryptorchidism.[19] This may imply the presence of placental hypoplasia and resultant chorionic gonadotropin deficiency as an underlying factor for genital anomalies.[11] In support of this notion, imprinted genes are known to play a pivotal role in body and placental growth,[20] and SRS is often associated with oligohydramnios, placental hypoplasia and undermasculinization.[11,21]

Genetic heterogeneity in IMAGe syndrome

Molecular data in case 3 imply the presence of genetic heterogeneity in IMAGe syndrome. Indeed, there was neither demonstrable *CDKN1C* mutation nor evidence for increased *CDKN1C* expression, while a pathologic mutation leading to gain-of-function or